Structural Engineering and Mechanics, *Vol. 75, No. 6 (2020) 747-769*
DOI: https://doi.org/10.12989/sem.2020.75.6.747

Bending and free vibration analysis of laminated piezoelectric composite plates

Pengchong Zhang*[1,2], Chengzhi Qi[1,2a], Hongyuan Fang[3a] and Xu Sun[1b]

[1]School of Civil and Transportation Engineering, Beijing University of Civil Engineering and Architecture, Beijing 102616, China
[2]Beijing Advanced Innovation Center for Future Urban Design, Beijing University of Civil Engineering and Architecture, Beijing 100044, China
[3]College of Water Conservancy & Environmental Engineering, Zhengzhou University. Zhengzhou 450001, China

(Received July 2, 2019, Revised March 12, 2020, Accepted March 19, 2020)

Abstract. This paper provides a semi-analytical approach to investigate the variations of 3D displacement components, electric potential, stresses, electric displacements and transverse vibration frequencies in laminated piezoelectric composite plates based on the scaled boundary finite element method (SBFEM) and the precise integration algorithm (PIA). The proposed approach can analyze the static and dynamic responses of multilayered piezoelectric plates with any number of laminae, various geometrical shapes, boundary conditions, thickness-to-length ratios and stacking sequences. Only a longitudinal surface of the plate is discretized into 2D elements, which helps to improve the computational efficiency. Comparing with plate theories and other numerical methods, only three displacement components and the electric potential are set as the basic unknown variables and can be represented analytically through the transverse direction. The whole derivation is built upon the three dimensional key equations of elasticity for the piezoelectric materials and no assumptions on the plate kinematics have been taken. By virtue of the equilibrium equations, the constitutive relations and the introduced set of scaled boundary coordinates, three-dimensional governing partial differential equations are converted into the second order ordinary differential matrix equation. Furthermore, aided by the introduced internal nodal force, a first order ordinary differential equation is obtained with its general solution in the form of a matrix exponent. To further improve the accuracy of the matrix exponent in the SBFEM, the PIA is employed to make sure any desired accuracy of the mechanical and electric variables. By virtue of the kinetic energy technique, the global mass matrix of the composite plates constituted by piezoelectric laminae is constructed for the first time based on the SBFEM. Finally, comparisons with the exact solutions and available results are made to confirm the accuracy and effectiveness of the developed methodology. What's more, the effect of boundary conditions, thickness-to-length ratios and stacking sequences of laminae on the distributions of natural frequencies, mechanical and electric fields in laminated piezoelectric composite plates is evaluated.

Keywords: laminated piezoelectric composite plates; static bending responses; free vibration; the scaled boundary finite element method; the precise integration algorithm

1. Introduction

In piezoelectric materials, mechanical deformations may occur when electric loads are applied. Accordingly, electric fields can be produced under the action of mechanical forces. Owing to their unique mechanical and electric coupling characteristics, piezoelectric materials are extensively used in various modern technological fields, such as aerospace, high-speed automobile, civil engineering, navigation, nuclear and infrastructure industries. Usually utilized as the surface-bonded or embedded layers, piezoelectric materials can be conveniently integrated into laminated plates to fulfill specific requirements, which are known as smart plate structures. In order to effectively and adequately take advantage of the laminated composite plate structures composed of piezoelectric materials in engineering applications, an accurate description of the static bending responses and free vibration behaviors is necessary.

Due to the characteristics of the interconversion between the mechanical and electric variables, laminated piezoelectric plates have attracted the attention of many engineers and researchers. Numerous models and theories to predict the static bending behaviors have been proposed. Detailed literature reviews and systematic presentation of laminated plates with piezoelectric laminae can be found in literatures (Saravanos and Heyliger 1999, Benjeddou 2000, Wang and Yang 2000, Mackerle 2003, Kapuria *et al*. 2010). Heyliger (1994) offered an accurate solution to a four layered hybrid composite plate composed of elastic and piezoelectric materials subjected to mechanical loads and surface electric potential. Heyliger (1997) presented closed-form solutions of mechanical and electric fields along the thickness in the single layer, two and three layered piezoelectric plates. The analytical solutions of simply supported angle-ply multilayered plates with thermo-piezoelectric materials in the cylindrical bending were provided by Dube *et al*. (1998). Cheung and Jiang (2001) took advantage of the semi-analytical finite layer and spline finite layer approach to explore the bending behaviors of composite plates containing piezoelectric materials. Cen *et*

*Corresponding author, Ph.D., Lecturer
E-mail: zhangpengchong@bucea.edu.cn
[a] Ph.D. Professor
[b] Ph.D. Lecturer

 ISSN: 1225-4568 (Print), 1598-6217 (Online)

al. (2002) put forward a four nodded quadrilateral element to investigate the deformation rules of composite plates with surface bonded or embedded piezoelectric layers. Garção *et al*. (2004) made a comparison between several layerwise plate theories to solve mechanical and electric solutions in multilayered plates including composite and piezoelectric laminae. Lage *et al*. (2004) established a layerwise mixed finite element model to predict the change regulations of mechanical and electric variables in three and five layered piezoelectric composite square plates. Kapuria (2004) utilized the third order theory and the layerwise linear zig-zag approximation to examine the static responses of a hybrid cross-ply plate containing piezoelectric layers. Based on the first order shear deformation plate theory, Wu *et al*. (2004) investigated the bending behaviors of the three-layered square piezoelectric composite plates under the simply supported boundary condition. Based on the mixed variational statement, Carrera and Nali (2009) proposed a new kind of plate element to evaluate the static behaviors of laminated plates with bonded piezoelectric sensor or actuator layers. With the help of the improved third order zig-zag plate theory, Kapuria and Kulkarni (2009) further extended the quadrilateral element proposed by Kapuria and Kulkarni (2008) to carry out the static analysis of hybrid composite plates containing piezoelectric laminae under the action of pressure and electric potential. By virtue of the Reissner mixed variational theorem, a new plate model was proposed by Carrera *et al*. (2010a) to analyze the cross-thickness distributions of mechanical and electric variables in piezoelectric composite plates. With the aid of the unified formulation, Carrera and Robaldo (2010b) exploited a hierarchical plate element to study the bending behaviors of three-layer piezoelectric plates. Torres and Mendonça (2010a) incorporated the third order shear deformation theory and the layerwise plate theory to estimate the static responses of composite plates with piezoelectric actuators or sensors. Aided by a higher order shear and normal deformation theory and layerwise plate theory to model mechanical quantities and electric potential, Shiyekar and Kant (2011) investigated the distributions of mechanical and electric fields in laminated piezoelectric composite plates. Torres *et al*. (2011) combined the third order shear deformation plate theory and the layerwise theory to simulate the static responses of multilayered plates coated or embedded piezoelectric sensors or actuators. Moleiro *et al*. (2012) utilized a new layerwise mixed least-squares model to study the flexural bending responses of laminated piezoelectric composite plates subjected to pressures and potential forces. Khandelwal *et al*. (2013) derived two-dimensional finite element plate model to investigate the static behaviors of laminated composite plates covered by piezoelectric materials. Kulikov and Plotnikova (2013) applied the sampling surfaces method to conduct the static analysis of laminated piezoelectric orthotropic plates, piezoelectric plates in cylindrical bending and antisymmetric piezoelectric angle-ply plates. By dint of the Mindlin's first order shear deformation theory, Rezaiee-Pajand and Sadeghi (2013) introduced a new triangular finite element to solve the bending problem of laminated composite plates containing piezoelectric layers. Built upon the third order shear deformation plate theory of Reddy, Li *et al*. (2014) used the bidirectional B-spline finite element method to study the parameter identification problem of laminated composite plates with piezoelectric materials. Moleiro *et al*. (2014) further developed the works of Heyliger (1994, 1997) and offered more benchmark examples on the static analysis of two, three and four layered piezoelectric composite plates with PVDF materials. Based on the least squares formulation, Moleiro *et al*. (2015) compared results of displacements, stresses, electric potential and electric displacements in three and four layered piezoelectric plates between two layerwise mixed models. Pendhari *et al*. (2015) gave out a simple two-dimensional semi-analytical solutions for the bending analysis of piezoelectric laminate under the cylindrical bending subjected to mechanical and electric loads. Plagianakos and Papadopoulos (2015) took advantage of the two and three-dimensional layerwise plate theories to analyze the static deformations of composite plates bonded with piezoelectric materials. Sawarkar *et al*. (2016) developed a semi-analytical model to analyze the through-thickness variations of mechanical and electric variables in multilayered piezoelectric plates under the simply supported boundary condition. With the help of the variable separation method, Vidal *et al*. (2016) carried out a study on the bending analysis of laminated piezoelectric composite plates subjected to mechanical pressure or electric potential.

The dynamic responses of structures are crucial for the design and performance evaluation (Li *et al* 2018, Li *et al*. 2019). So many studies focus on the free vibration behaviors of laminated piezoelectric plates. Heyliger and Brooks (1995a) acquired the vibration frequencies and mode shapes of single layer, two layered, three-ply hybrid and three layered piezoelectric plates under the cylindrical bending. Built upon the linear theory, exact solutions of natural frequencies and modes for laminated piezoelectric composite plates were obtained by Heyliger and Saravanos (1995b). Saravanos *et al*. (1997) applied laminate theories to present the vibration characteristics of laminated composite plates containing piezoelectric layers. By means of the state space method and the finite Hankel transform, the eigenvalues of a laminated circular plate with transversely isotropic and piezoelectric materials were evaluated by Ding *et al*. (1997). Heyliger and Ramirez (2000) took advantage of the discrete layer method to present the free vibration behaviors of a multilayered circular plate containing elastic and piezoelectric layers. Based on the Mindlin plate theory, Benjeddou and Deü (2002a) obtained the elastic solutions of natural frequencies for laminated piezoelectric composite plates under the simply supported boundary condition. Benjeddou *et al*. (2002b) utilized the layerwise first order shear deformation theory in conjunction with the quadratic non-uniform electric potential to analyze the dynamic behaviors of simply-supported piezoelectric adaptive composite plates. Vel *et al*. (2004) made use of the Stroh formalism to determine the cylindrical bending vibration frequencies and mode shapes of layered plates with either surface mounted or embedded piezoelectric patches. With the aid of

Kirchhoff and Mindlin plate theory, Duan *et al*. (2005) made a research on the free vibration characteristics of three layered piezoelectric annular plate. Bian *et al*. (2006) took advantage of the state space formulations to study the static and dynamic responses of composite plates comprised by the functionally graded surface layers and homogeneous piezoelectric core layer and utilized the spring layer model to simulate the weak interfaces. Based on the differential quadrature, Zhang *et al*. (2006) proposed a three dimensional model to solve the natural frequencies of laminated piezoelectric plates. With the help of Lagrangian polynomials, Akhras and Li (2007) employed a finite layer method to study the static, free vibration and stability responses of the multilayered plate containing elastic and piezoelectric lamina. Balamurugan and Narayanan (2007) brought forward a higher order, field consistent and shear flexible plate model to investigate the static and dynamic behaviors of piezoelectric laminates. Liu *et al*. (2008) introduced a finite element model to simulate the three dimensional axisymmetric and non-axisymmetric free vibration responses of multilayered circular and annular plates with piezoelectric layers. Hashemi *et al*. (2010) applied a new model based on the Levinson plate theory to analyze the free vibration behaviors of three layered piezoelectric annular plate under kinds of boundary conditions and further demonstrated the effect of plate parameters and piezoelectric layer on natural frequencies. Hosseini-Hashemi *et al*. (2010) exploited the third order shear deformation plate theory of Reddy, Hamiltonian and minimum potential energy principles to gain analytical solutions of transverse vibration for thick piezoelectric annular plates. Torres and Paulo (2010b) mixed the equivalent single layer and the layerwise plate theory to carry out the static bending and free vibration analysis of hybrid composite plates with piezoelectric layers. By virtue of the Kirchhoff plate theory and the Maxwell equation, Wu *et al*. (2010) developed an accurate and efficient model to compute vibration frequencies and mode shapes of a laminated piezoelectric circular plate with the open circuit electric surface boundary condition. Akhras and Li (2011) took advantage of a spline finite strip approach coupled with the Reddy's third order shear deformation theory to provide the eigensolutions and buckling loads of hybrid piezoelectric plates. Khandelwal *et al*. (2014) employed a new C0 two dimensional finite element plate model to study the static and dynamic responses of composite plates including piezoelectric laminae under the action of mechanical loads or electric potential. Based on the systematic power series expansion method, Mauritsson and Folkow (2015) provided dispersion curves and vibration frequencies of single and laminated piezoelectric plates with various thickness-to-length ratios. Messina and Carrera (2015) made use of a displacement-based variational statement and the transfer matrix approach to study the free vibration behaviors of laminated piezoelectric composite plates under different boundary conditions. Aided by a set of adaptive global piecewise smooth functions, Messina and Carrera (2016) conducted a study on the vibration responses of laminated piezoelectric composite plates. By virtue of the first order shear deformation theory, Ghasemabadian and Saidi (2017) solved the critical buckling loads and mode number of multilayered rectangular plates with the piezoelectric laminae. Moleiro *et al*. (2017) derived the exact solutions of natural frequencies and through-thickness distributions of mode shapes for three and four layered piezoelectric composite plates. Kulikov and Plotnikova (2017) adopted the sampling method to analyze the free vibration behaviors of single and hybrid four layered piezoelectric square plates. Singh *et al*. (2017) studied the influences of the interface imperfection on the propagation behaviors of the Love-type wave in the fiber-reinforced half-space bonded with the piezoelectric layer. Askari *et al*. (2018) employed the Mindlin plate theory to investigate the dynamic responses of rectangular porous composite plates coated with piezoelectric layers. By means of the first order shear deformation theory and the Hamilton's principle, Baghaee *et al*. (2019) utilized the Legendre polynomial series and the Lagrange multipliers to solve the eigensolutions of multilayered rectangular piezoelectric composite plates under different boundary conditions. With the help of the equivalent single layer plate theory, Tanzadeh and Amoushahi (2019) applied the finite strip method to conduct the free vibration and buckling analysis of multilayered composite plates with piezoelectric materials.

Alternatively, as a semi-analytical approach, the SBFEM is utilized to study the static and dynamic responses of laminated piezoelectric composite plates in this work. As a promising numerical method, the SBFEM proposed by Wolf and Song (1997, 2000a,b) only needs to discretize the boundary of the research domain, which is similar with the boundary element method (BEM) and contributes to improving the computational effectiveness. However, the fundamental solutions are not necessary in the SBFEM. Moreover, the SBFEM is analytical along the radial direction and can obtain solutions of the finite element method (FEM) sense in the circumferential direction. Until now, the SBFEM has been applied to many research areas, such as the soil-structure-interaction (Song 2009, Chen *et al*. 2014), heat transfer (Song 1999, Birk and Song 2009) and cracked problems (Song *et al*. 2010, Li *et al*. 2014). Recently, researchers have successfully exploited the SBFEM to analyze the bending behaviors and dynamic characteristics of beams (Li *et al*. 2017), elastic plates (Man *et al*. 2012, 2013), laminated composite plates (Lin *et al*. 2018), functionally graded plates (Xiang *et al*. 2014, Zhang *et al*. 2020), piezoelectric (Man *et al*. 2014) and magneto-electric-elastic plates (Zhang *et al*. 2019).

From the preceding literature overview, it can be seen that the SBFEM has many advantages over the traditional FEM and BEM. But to the best of the authors' knowledge, there is no paper concerning the bending and free vibration analysis of multilayered piezoelectric plates utilizing the SBFEM. This is where the present article comes to fill this gap. And its accuracy still needs to be improved in solving the matrix exponent. To further increase the accuracy of the matrix exponent in the SBFEM, the PIA (Zhong *et al*. 2004) is utilized to make sure any desired accuracy. Meanwhile, for the first time this article provides the global mass matrix of the laminated piezoelectric composite plates based on the SBFEM.

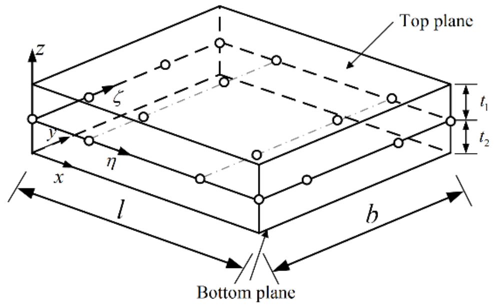

(a) A typical two layered piezoelectric plate

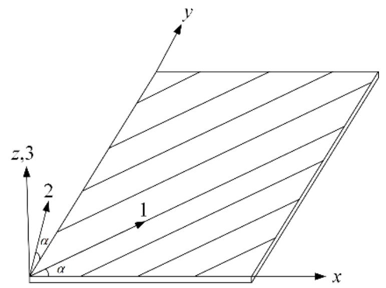

(b) (1,2,3) reference axes and (x,y,z) reference axes

Fig. 1 A model of the laminated piezoelectric composite plate

In the SBFEM, only a surface parallel with the bottom or top plane is demanded to be discretized with two dimensional elements, which is helpful to improve the computational efficiency. The high order spectral elements are adopted to accurately simulate the plates with curved boundaries. Moreover, only three elastic displacements and the electric potential are selected as the primary unknown variables and can be formulated analytically along the transverse direction. To improve the accuracy of natural frequencies, mechanical and electric quantities, the PIA is exploited to solve the matrix exponent to make sure high accuracy. The paper is organized as follows. The detailed theoretical derivations of the SBFEM governing equation are shown in Section 2. The Section 3 mainly introduces the solution procedure of the global stiffness matrix for the composite plate. The Section 4 establishes the global mass matrix of the laminated piezoelectric plate. Several numerical examples of three, four and five layered piezoelectric plates are provided in Section 5. Finally, the conclusion is presented in Section 6.

2. Governing equation of the laminated piezoelectric plate

In this section, detailed derivations of the governing equation for the laminated piezoelectric plates based on the SBFEM are presented. Only a longitudinal surface of the multilayered piezoelectric plate needs to be discretized with 2D elements, which helps to improve the computational efficiency. Meanwhile, the 3D displacement field and the electric potential along the thickness are expressed analytically. The PIA is introduced to make sure any desired accuracy. The geometry of a two layered piezoelectric plate and one of the laminae are shown in Fig. 1. In piezoelectric plates, the translational displacements along the x, y and z directions and the electric potential are selected as the fundamental unknown quantities. Expressions of $u_x=u_x(x,y,z)$, $u_y=u_y(x,y,z)$ and $u_z=u_z(x,y,z)$ are elastic displacement components and $\Phi=\Phi(x,y,z)$ is the electric potential of a point (x,y,z) in the piezoelectric plate. In order to facilitate the analysis, a generalized variable $\{\bar{u}\} = \{\bar{u}(x,y,z)\} = [u_z \quad u_x \quad u_y \quad \Phi]^T$ is defined. It is necessary to indicate that the piezoelectric plate is meshed by the spectral elements. In the spectral element, the Gauss-Lobatto-Legendre (GLL) quadrature instead of the conventional Gauss quadrature is utilized. Integration points coincide with the locations of the field nodes, which contributes to simplifying some coefficient matrices into lumped ones. Utilization of the high-order spectral elements is helpful to increase the computational efficiency.

The relationships between the elastic strain ε_{ij}, the electric field E_i and the displacement field, the electric potential in the tensor form are shown as

$$\varepsilon_{ij} = \frac{1}{2}\left(u_{j,i} + u_{i,j}\right) \tag{1}$$

$$-E_i = \Phi_{,i} \tag{2}$$

By introducing the differential operator $[L]$

$$[L]=\begin{bmatrix} \frac{\partial}{\partial z} & 0 & 0 & 0 & \frac{\partial}{\partial y} & \frac{\partial}{\partial x} & 0 & 0 & 0 \\ 0 & \frac{\partial}{\partial x} & 0 & \frac{\partial}{\partial y} & 0 & \frac{\partial}{\partial z} & 0 & 0 & 0 \\ 0 & 0 & \frac{\partial}{\partial y} & \frac{\partial}{\partial x} & \frac{\partial}{\partial z} & 0 & 0 & 0 & 0 \\ 0 & 0 & 0 & 0 & 0 & 0 & \frac{\partial}{\partial z} & \frac{\partial}{\partial x} & \frac{\partial}{\partial y} \end{bmatrix}^T \tag{3}$$

the strain and electric field $\{\bar{\varepsilon}\} = \{\bar{\varepsilon}(x,y,z)\}$ is expressed as

$$\begin{aligned}\{\bar{\varepsilon}\} &= \begin{bmatrix} \varepsilon_{zz} & \varepsilon_{xx} & \varepsilon_{yy} & \gamma_{xy} & \gamma_{yz} & \gamma_{xz} & -E_z & -E_x & -E_y \end{bmatrix}^T \\ &= [L]\{\bar{u}\}\end{aligned} \tag{4}$$

The constitutive law of the piezoelectric material with reference to the local fiber coordinate system (3-1-2) as shown in Fig. 1 can be formulated as

$$\begin{bmatrix} \sigma_{33} \\ \sigma_{11} \\ \sigma_{22} \\ \tau_{12} \\ \tau_{23} \\ \tau_{13} \\ D_3 \\ D_1 \\ D_2 \end{bmatrix} = \begin{bmatrix} c_{33} & c_{13} & c_{23} & 0 & 0 & 0 & e_{33} & 0 & 0 \\ c_{13} & c_{11} & c_{12} & 0 & 0 & 0 & e_{31} & 0 & 0 \\ c_{13} & c_{12} & c_{22} & 0 & 0 & 0 & e_{32} & 0 & 0 \\ 0 & 0 & 0 & c_{45} & 0 & 0 & 0 & 0 & 0 \\ 0 & 0 & 0 & 0 & c_{56} & 0 & 0 & 0 & e_{24} \\ 0 & 0 & 0 & 0 & 0 & c_{46} & 0 & e_{15} & 0 \\ e_{33} & e_{31} & e_{31} & 0 & 0 & 0 & -\nu_{33} & 0 & 0 \\ 0 & 0 & 0 & 0 & 0 & e_{15} & 0 & -\nu_{11} & 0 \\ 0 & 0 & 0 & 0 & e_{24} & 0 & 0 & 0 & -\nu_{22} \end{bmatrix} \begin{bmatrix} \varepsilon_{33} \\ \varepsilon_{11} \\ \varepsilon_{22} \\ \gamma_{12} \\ \gamma_{23} \\ \gamma_{31} \\ -E_3 \\ -E_1 \\ -E_2 \end{bmatrix} = [C] \begin{bmatrix} \varepsilon_{33} \\ \varepsilon_{11} \\ \varepsilon_{22} \\ \gamma_{12} \\ \gamma_{23} \\ \gamma_{13} \\ -E_3 \\ -E_1 \\ -E_2 \end{bmatrix} \tag{5}$$

in which $[\sigma_{33}\ \sigma_{11}\ \sigma_{22}\ \tau_{12}\ \tau_{23}\ \tau_{13}\ D_3\ D_1\ D_2]$ represent the stresses and electric displacements; c_{ij}, e_{ij}, ν_{ij} stand for elastic stiffness, piezoelectric and dielectric coefficients in the local fiber coordinate system (3-1-2).

Transforming stresses, electric displacements, strains, electric fields from the local fiber coordinate system (3-1-2) to the Cartesian coordinate system *z*–*x*–*y*, the constitutive relations in the Cartesian coordinate system can be written as

$$\begin{aligned}\{\bar{\sigma}\} &= \begin{bmatrix}\sigma_{zz} & \sigma_{xx} & \sigma_{yy} & \tau_{xy} & \tau_{yz} & \tau_{xz} & D_z & D_x & D_y\end{bmatrix}^T \\ &= [Q]\{\bar{\varepsilon}\}\end{aligned} \tag{6}$$

where

$$[Q]=\begin{bmatrix} Q_{33} & Q_{13} & Q_{23} & Q_{34} & 0 & 0 & \bar{e}_{33} & 0 & 0 \\ Q_{13} & Q_{11} & Q_{12} & Q_{14} & 0 & 0 & \bar{e}_{31} & 0 & 0 \\ Q_{23} & Q_{12} & Q_{22} & Q_{24} & 0 & 0 & \bar{e}_{32} & 0 & 0 \\ Q_{34} & Q_{14} & Q_{24} & Q_{44} & 0 & 0 & \bar{e}_{34} & 0 & 0 \\ 0 & 0 & 0 & 0 & Q_{55} & Q_{66} & 0 & \bar{e}_{15} & \bar{e}_{25} \\ 0 & 0 & 0 & 0 & Q_{56} & Q_{66} & 0 & \bar{e}_{16} & \bar{e}_{26} \\ \bar{e}_{33} & \bar{e}_{31} & \bar{e}_{32} & \bar{e}_{34} & 0 & 0 & -\nu_{zz} & 0 & 0 \\ 0 & 0 & 0 & 0 & \bar{e}_{15} & \bar{e}_{16} & 0 & -\nu_{xx} & -\nu_{xy} \\ 0 & 0 & 0 & 0 & \bar{e}_{25} & \bar{e}_{26} & 0 & -\nu_{xy} & -\nu_{yy} \end{bmatrix} \tag{7}$$

$[\sigma_{zz}\ \sigma_{xx}\ \sigma_{yy}\ \tau_{xy}\ \tau_{yz}\ \tau_{xz}\ D_z\ D_x\ D_y]^T$ and $[\varepsilon_{zz}\ \varepsilon_{xx}\ \varepsilon_{yy}\ \gamma_{xy}\ \gamma_{yz}\ \gamma_{xz}\ \text{-}E_z\ \text{-}E_x\ \text{-}E_y]^T$ are the stress, electric displacement, strain and electric field components referred to the Cartesian coordinate system. What's more, $[Q]$ is the converted stiffness matrix of the piezoelectric material in the global coordinate system *z*–*x*–*y*. The detailed conversion from $[C]$ to $[Q]$ are illustrated in the appendix (Akhras and Li 2007).

The key equilibrium equations ignoring the body force and electric charge for piezoelectric materials can be formulated as

$$\frac{\partial \sigma_{xx}}{\partial x}+\frac{\partial \tau_{xy}}{\partial y}+\frac{\partial \tau_{xz}}{\partial z}=0 \tag{8}$$

$$\frac{\partial \tau_{xy}}{\partial x}+\frac{\partial \sigma_{yy}}{\partial y}+\frac{\partial \tau_{yz}}{\partial z}=0 \tag{9}$$

$$\frac{\partial \tau_{xz}}{\partial x}+\frac{\partial \tau_{yz}}{\partial y}+\frac{\partial \sigma_{zz}}{\partial z}=0 \tag{10}$$

$$\frac{\partial D_x}{\partial x}+\frac{\partial D_y}{\partial y}+\frac{\partial D_z}{\partial z}=0 \tag{11}$$

Aided by the differential operator $[L]$, Eqs. (8-11) can be simplified as

$$[L]^T\{\bar{\sigma}\}=0 \tag{12}$$

A set of the scaled boundary coordinates η and ζ is introduced to convert the governing partial differential equations into an ordinary differential matrix one. In the process, only a longitudinal surface of the laminated piezoelectric plate needs to be discretized with two-dimensional spectral elements. For example, the nodal locations of the third order spectral element in a typical two-layered plate are plotted in Fig. 1. The scaling center O is set at the infinity. $\{x\}$ and $\{y\}$ in the global coordinate system are employed to represent the nodal coordinates of the discretized mesh. The coordinates $(x(\eta,\zeta), y(\eta,\zeta))$ of any node in the discretized plane can be interpolated utilizing the shape function $[N]=[N(\eta,\zeta)]=[N_1((\eta,\zeta))\ N_2((\eta,\zeta))\ \ldots]$.

$$\begin{aligned} x(\eta,\zeta) &= [N]\{x\} \\ y(\eta,\zeta) &= [N]\{y\} \end{aligned} \tag{13}$$

The transformation from the scaled boundary coordinates to the Cartesian coordinate system can be expressed as

$$\begin{Bmatrix} \partial/\partial\eta \\ \partial/\partial\zeta \end{Bmatrix} = \mathbf{J}(\eta,\zeta) \begin{Bmatrix} \partial/\partial x \\ \partial/\partial y \end{Bmatrix} \tag{14}$$

The Jacobian matrix is denoted as

$$\mathbf{J}(\eta,\zeta)=\begin{bmatrix} [N]_{,\eta}\{x\} & [N]_{,\eta}\{y\} \\ [N]_{,\zeta}\{x\} & [N]_{,\zeta}\{y\} \end{bmatrix} = \begin{bmatrix} x_{,\eta} & y_{,\eta} \\ x_{,\zeta} & y_{,\zeta} \end{bmatrix} \tag{15}$$

and its determinant is formulated as

$$|\mathbf{J}(\eta,\zeta)| = x_{,\eta}y_{,\zeta} - y_{,\eta}x_{,\zeta} \tag{16}$$

By virtue of $\begin{Bmatrix} \partial/\partial x \\ \partial/\partial y \end{Bmatrix} = \boldsymbol{J}(\eta,\zeta)^{-1} \begin{Bmatrix} \partial/\partial\eta \\ \partial/\partial\zeta \end{Bmatrix}$ and with respect to the scaled boundary coordinates η and ζ, the differential operator $[L]$ in Eq. (3) can be rewritten as

$$[L]=[b^1]\frac{\partial}{\partial z}+[b^2]\frac{\partial}{\partial \eta}+[b^3]\frac{\partial}{\partial \zeta} \tag{17}$$

where coefficient matrices $[b^1]$, $[b^2]$ and $[b^3]$ are denoted as

$$[b^1]=\begin{bmatrix} 1 & 0 & 0 & 0 \\ 0 & 0 & 0 & 0 \\ 0 & 0 & 0 & 0 \\ 0 & 0 & 0 & 0 \\ 0 & 0 & 1 & 0 \\ 0 & 1 & 0 & 0 \\ 0 & 0 & 0 & 1 \\ 0 & 0 & 0 & 0 \\ 0 & 0 & 0 & 0 \end{bmatrix} \quad [b^2]=\frac{1}{|J|}\begin{bmatrix} 0 & 0 & 0 & 0 \\ 0 & y_{,\zeta} & 0 & 0 \\ 0 & 0 & -x_{,\zeta} & 0 \\ 0 & -x_{,\zeta} & y_{,\zeta} & 0 \\ -x_{,\zeta} & 0 & 0 & 0 \\ y_{,\zeta} & 0 & 0 & 0 \\ 0 & 0 & 0 & 0 \\ 0 & 0 & 0 & y_{,\zeta} \\ 0 & 0 & 0 & -x_{,\zeta} \end{bmatrix} \quad [b^3]=\frac{1}{|J|}\begin{bmatrix} 0 & 0 & 0 & 0 \\ 0 & -y_{,\eta} & 0 & 0 \\ 0 & 0 & x_{,\eta} & 0 \\ 0 & x_{,\eta} & -y_{,\eta} & 0 \\ x_{,\eta} & 0 & 0 & 0 \\ -y_{,\eta} & 0 & 0 & 0 \\ 0 & 0 & 0 & 0 \\ 0 & 0 & 0 & -y_{,\eta} \\ 0 & 0 & 0 & x_{,\eta} \end{bmatrix} \tag{18}$$

The vector of the elastic displacements and electric potential $\{\bar{u}(z,\eta,\zeta)\}$ at any point in the discretized plane can be acquired with the help of the shape function matrix $[\boldsymbol{N}]$.

$$\{\bar{u}(z,\eta,\zeta)\}=\begin{bmatrix} [N] & [0] & [0] & [0] \\ [0] & [N] & [0] & [0] \\ [0] & [0] & [N] & [0] \\ [0] & [0] & [0] & [N] \end{bmatrix}\begin{bmatrix} \{u_z(z)\} \\ \{u_x(z)\} \\ \{u_y(z)\} \\ \{\Phi(z)\} \end{bmatrix}=[\mathbf{N}]\{\bar{u}(z)\} \tag{19}$$

From Eqs. (4), (17) and (19), the following formulation can be obtained.

$$\{\bar{\varepsilon}\} = \left[B^1\right]\{\bar{u}(z)\}_{,z} + \left[B^2\right]\{\bar{u}(z)\} \tag{20}$$

in which $[B^1]$ and $[B^2]$ are expressed as $[B^1] = [b^1][\boldsymbol{N}]$ and $[B^2] = [b^2][\boldsymbol{N}]_{,\eta} + [b^3][\boldsymbol{N}]_{,\zeta}$.

According to Eqs. (6) and (20), the stress field for the piezoelectric material is denoted as

$$\{\bar{\sigma}\} = [Q](\left[B^1\right]\{\bar{u}(z)\}_{,z} + \left[B^2\right]\{\bar{u}(z)\}) \tag{21}$$

Built upon the virtual work principle and a series of relevant derivations, the SBFEM governing ordinary differential equation with respect to $\{\bar{u}(z)\}$ for the laminated piezoelectric composite plates can be gained.

$$[E^0]\{\bar{u}(z)\}_{,zz} + ([E^1]^T - [E^1])\{\bar{u}(z)\}_{,z} - [E^2]\{\bar{u}(z)\} = 0 \tag{22}$$

where $[E^0]$, $[E^1]$ and $[E^2]$ are coefficient matrices.

$$[E^0] = \int_{-1}^{1}\int_{-1}^{1}[B^1]^T[Q][B^1]|J|\,d\eta d\zeta \tag{23}$$

$$[E^1] = \int_{-1}^{1}\int_{-1}^{1}[B^2]^T[Q][B^1]|J|\,d\eta d\zeta \tag{24}$$

$$[E^2] = \int_{-1}^{1}\int_{-1}^{1}[B^2]^T[Q][B^2]|J|\,d\eta d\zeta \tag{25}$$

In the above derivation, only the necessary formulae related to the process of derivation are introduced. Further details are listed in articles (Man *et al.* 2012, Man *et al.* 2013). To facilitate the exhibition of the derivation process, only one element of the SBFEM is shown as an example. It is essential to assemble all elements similar with the FEM to model the whole plate.

3. Solution procedure of the SBFEM governing equation

Except for the Taylor series and Padé expansion, this article introduces a new method named the PIA to present the solution procedure of the SBFEM governing equation. As a highly accurate method, the PIA is utilized to make sure any desired accuracy of the mechanical and electric variables in the laminated piezoelectric plates.

At first, an internal nodal force served as the dual vector of $\{\bar{u}(z)\}$ is proposed.

$$\{\bar{q}(z)\} = \left[E^0\right]\{\bar{u}(z)\}_{,z} + \left[E^1\right]^T\{\bar{u}(z)\} \tag{26}$$

By dint of the vector $\{X(z)\} = \{\{\bar{u}(z)\} \quad \{\bar{q}(z)\}\}^T$, a reduced first order ordinary differential equation can be obtained.

$$\{X(z)\}_{,z} = -[Z]\{X(z)\} \tag{27}$$

in which the matrix $[Z]$ is denoted as

$$[Z] = \begin{bmatrix} \left[E^0\right]^{-1}\left[E^1\right]^T & -\left[E^0\right]^{-1} \\ -\left[E^2\right] + \left[E^1\right]\left[E^0\right]^{-1}\left[E^1\right]^T & -\left[E^1\right]\left[E^0\right]^{-1} \end{bmatrix} \tag{28}$$

It's convenient to solve Eq. (27) and its general solution is formulated as

$$\{X(z)\} = e^{-[Z]z}\{c\} \tag{29}$$

In Eq. (29), $e^{-[Z]z}$ is a matrix exponent which is calculated by the PIA in this paper. $\{c\}$ is the integration constant vector, which is determined by the boundary conditions.

The ith lamina with the thickness t_i in the multilayered piezoelectric plate is shown as an example and the following expression can be acquired.

$$\{X_B\} = \{c\} \qquad \{X_T\} = e^{-[Z]t_i}\{c\} = \exp(-[Z]t_i)\{c\} \tag{30}$$

in which $\{X_B\}$ and $\{X_T\}$ represent the dual vectors at the bottom and top planes of the ith lamina.

Meanwhile, Eq. (30) can be expressed as

$$\begin{Bmatrix}\{\bar{u}_B\}\\ \{\bar{q}_B\}\end{Bmatrix} = \begin{Bmatrix}\{\bar{u}_B\}\\ -\{F_B\}\end{Bmatrix} = \begin{Bmatrix}\{c_1\}\\ \{c_2\}\end{Bmatrix} \quad \begin{Bmatrix}\{\bar{u}_T\}\\ \{\bar{q}_T\}\end{Bmatrix} = \begin{Bmatrix}\{\bar{u}_T\}\\ \{F_T\}\end{Bmatrix} = \exp(-[Z]t_i)\begin{Bmatrix}\{c_1\}\\ \{c_2\}\end{Bmatrix} \tag{31}$$

where $\{F_B\}$ and $\{F_T\}$ are the external forces applied on the bottom and top planes of this lamina.

By virtue of the PIA, the thickness t_i of this lamina is divided into 2^N sub-layers with the equal thickness ξ. The thickness of a sub-layer ξ is extremely small and the corresponding matrix exponent can be formulated in terms of the fourth order Taylor's expansion to ensure enough accuracy.

$$\begin{aligned}\{X_T\} &= \exp(-[Z]t_i/2^N)^{2^N}\{c\} = \exp(-[Z]\xi)^{2^N}\{c\} \\ &= \mathbf{T}^{2^N}\{c\} = \bar{\mathbf{T}}\{c\}\end{aligned} \tag{32}$$

with $\boldsymbol{T} = exp(-[Z]\xi)$ and $\bar{\boldsymbol{T}} = \boldsymbol{T}^{2^N}$.

In the above formulation, $\boldsymbol{T}$ can be computed by

$$\begin{aligned}&\mathbf{T} = \exp(-[Z]\xi) \approx \mathbf{I} + \mathbf{T}_a \\ &\mathbf{T}_a = (-[Z]\xi) + \frac{1}{2!}(-[Z]\xi)^2 + \frac{1}{3!}(-[Z]\xi)^3 + \frac{1}{4!}(-[Z]\xi)^4\end{aligned} \tag{33}$$

in which $\boldsymbol{I}$ is a unit matrix

The estimation of $\bar{\boldsymbol{T}}$ is conducted by the following successive factorization.

$$\bar{\mathbf{T}} = (\mathbf{I} + \mathbf{T}_a)^{2^N} = (\mathbf{I} + \mathbf{T}_a)^{2^{N-1}} \times (\mathbf{I} + \mathbf{T}_a)^{2^{N-1}} = \mathbf{I} + \mathbf{T}_r^N \tag{34}$$

Through the recursive formulation N times as follows, $\boldsymbol{T}_r^N$ can be denoted as

$$\begin{aligned}&\mathbf{T}_r^i = 2\mathbf{T}_r^{i-1} + \mathbf{T}_r^{i-1} \times \mathbf{T}_r^{i-1} \quad (i = 1, 2, \ldots, N) \\ &\mathbf{T}_r^0 = \mathbf{T}_a\end{aligned} \tag{35}$$

in which $\boldsymbol{T}_a$ is estimated by Eq. (33). In the above computations, the standard algebraic matrix operations are adopted, which helps to reduce the calculation time.

From Eqs. (31) and (32), the following expression can be gained.

$$\begin{Bmatrix}\{\bar{u}_T\}\\ \{F_T\}\end{Bmatrix} = \bar{\mathbf{T}}\begin{Bmatrix}\{c_1\}\\ \{c_2\}\end{Bmatrix} = \begin{bmatrix}\bar{\mathbf{T}}_{11} & \bar{\mathbf{T}}_{12}\\ \bar{\mathbf{T}}_{21} & \bar{\mathbf{T}}_{22}\end{bmatrix}\begin{Bmatrix}\{c_1\}\\ \{c_2\}\end{Bmatrix}$$
$$= \begin{bmatrix}\bar{\mathbf{T}}_{11} & \bar{\mathbf{T}}_{12}\\ \bar{\mathbf{T}}_{21} & \bar{\mathbf{T}}_{22}\end{bmatrix}\begin{Bmatrix}\{\bar{u}_B\}\\ -\{F_B\}\end{Bmatrix} \tag{36}$$

Grouping the unknown variables and the imposed external forces to each side of the Eq. (36), the stiffness equation for the *i*th piezoelectric lamina is formulated as

$$[k]\begin{Bmatrix}\{\bar{u}_B\}\\ \{\bar{u}_T\}\end{Bmatrix} = \begin{Bmatrix}\{F_B\}\\ \{F_T\}\end{Bmatrix} \tag{37}$$

where the stiffness matrix [*k*] is shown as

$$[k] = \begin{bmatrix}\bar{\mathbf{T}}_{12}^{-1}\bar{\mathbf{T}}_{11} & -\bar{\mathbf{T}}_{12}^{-1}\\ \bar{\mathbf{T}}_{21} - \bar{\mathbf{T}}_{22}\bar{\mathbf{T}}_{12}^{-1}\bar{\mathbf{T}}_{11} & \bar{\mathbf{T}}_{22}\bar{\mathbf{T}}_{12}^{-1}\end{bmatrix} \tag{38}$$

Similar with the foregoing derivations, it's convenient to obtain the stiffness matrix of each lamina. In view of the compatible and continuous boundary conditions at interfaces in the laminated piezoelectric composite plates, the global stiffness equation of the *N*-layered piezoelectric plate can be assembled in the following.

$$\begin{Bmatrix}F_1\\ F_2\\ F_3\\ .\\ .\\ F_{i+1}\\ F_{i+2}\\ .\\ .\\ F_N\end{Bmatrix} = \begin{bmatrix}k_{11}^1 & k_{12}^1 & 0 & . & . & 0 & 0 & . & . & 0\\ k_{21}^1 & k_{22}^1+k_{11}^2 & k_{12}^2 & & & & & & & 0\\ 0 & k_{21}^2 & k_{22}^2+k_{11}^3 & & & & & & & 0\\ . & & & & . & & & & & .\\ . & & & & & . & & & & .\\ 0 & & . & . & & k_{22}^i+k_{11}^{i+1} & k_{12}^{i+1} & & & 0\\ 0 & & . & . & & k_{21}^{i+1} & k_{22}^{i+1}+k_{11}^{i+2} & & & 0\\ . & & & & & & & . & & .\\ . & & & & & & & & & k_{12}^N\\ 0 & & . & . & & 0 & 0 & . & k_{21}^N & k_{22}^N\end{bmatrix}\begin{Bmatrix}U_1\\ U_2\\ U_3\\ .\\ .\\ U_{i+1}\\ U_{i+2}\\ .\\ .\\ U_N\end{Bmatrix} \tag{39}$$

in which the matrix elements k_{11}^i, k_{12}^i, k_{21}^i and k_{22}^i demonstrate the stiffness of the *i*th-lamina (*i*=1,2,...*N*) in the multilayered piezoelectric plate.

Eq. (39) can be abbreviated as

$$\{F\} = [K]\{U\} \tag{40}$$

with the global stiffness matrix [*K*].

4. Mass Matrix of the laminated piezoelectric plate

To investigate the free vibration characteristics, for the first time the global mass matrix of the laminated piezoelectric composite plates is given out based on the SBFEM in this paper. Following the solution procedure of the stiffness matrix, the mass matrix for the *i*th-lamina is shown as an example.

The kinetic energy δK for the *i*th-lamina is denoted as

$$\delta K = \int_V \delta\bar{u}(z)^T[\mathbf{N}]^T\rho^{(i)}\begin{bmatrix}1 & & & \\ & 1 & & \\ & & 1 & \\ & & & 0\end{bmatrix}[\mathbf{N}]\ddot{\bar{u}}(z)dV \tag{41}$$

in which $\rho^{(i)}$ is the mass density and $\ddot{u}(z)$ is the acceleration vector.

Substituting $dV = |J|d\eta d\zeta dz$ into Eq. (41), the following formula can be obtained

$$\delta K = \int \delta\bar{u}(z)^T\left(\int_S[\mathbf{N}]^T\rho^{(i)}\begin{bmatrix}1 & & & \\ & 1 & & \\ & & 1 & \\ & & & 0\end{bmatrix}[\mathbf{N}]|J|d\eta d\zeta\right)\ddot{\bar{u}}(z)dz \tag{42}$$

According to Eq. (42), the mass matrix for the *i*th-lamina is established as

$$\left[m^i\right] = \begin{bmatrix}m_B^i & 0\\ 0 & m_T^i\end{bmatrix} \tag{43}$$

where m_B^i and m_T^i are derived as

$$m_B^i = m_T^i = \frac{t_i}{2}\int_S[\mathbf{N}]^T\rho^{(i)}\begin{bmatrix}1 & & & \\ & 1 & & \\ & & 1 & \\ & & & 0\end{bmatrix}[\mathbf{N}]|J|d\eta d\zeta \tag{44}$$

By virtue of the compatible and continuous boundary conditions, the global mass matrix for the multilayered piezoelectric plate is constructed as

$$[M] = \begin{bmatrix}m_B^1 & 0 & 0 & . & . & 0 & 0 & . & . & 0\\ 0 & m_T^1+m_B^2 & 0 & & & & & & & 0\\ 0 & 0 & m_T^2+m_B^3 & & & & & & & 0\\ . & & & & . & & & & & .\\ . & & & & & . & & & & .\\ 0 & . & . & & & m_T^i+m_B^{i+1} & 0 & & & 0\\ 0 & . & . & & & 0 & m_T^{i+1}+m_B^{i+2} & & & 0\\ . & & & & & & & . & & .\\ . & & & & & & & & m_T^{N-1}+m_B^N & 0\\ 0 & . & . & & & 0 & 0 & . & 0 & m_T^N\end{bmatrix} \tag{45}$$

Aided by the global mass matrix [*M*] and stiffness matrix [*K*] depicted in Eqs. (40) and (45) respectively, it's convenient to acquire the natural frequencies of the laminated piezoelectric composite plates.

5. Numerical examples

This section provides seven numerical examples to verify the accuracy and effectiveness of the proposed technique and discuss the influence of boundary conditions, thickness-to-length ratios and stacking sequence of laminae on the distributions of elastic displacements, electric potential, stresses, electric displacements and natural frequencies in laminated piezoelectric composite plates. The first four examples examine the static bending behaviors of the multilayered piezoelectric plates. The next three examples pay attention to the free vibration responses of the layered composite plates. In the first example, the plate is constituted by three cross-ply laminae. The second and third examples investigate the deformable responses of four layered piezoelectric plates. The fourth example studies the bending behaviors of a perforated plate. In the last three examples, the present procedure is utilized to evaluate the eigenvalues of three and five layered hybrid piezoelectric composite plates. All examples are conducted

Table 1 Material properties

	PVDF	PZT-4	Graphite-epoxy
c_{11} (GPa)	238.0	139.0	134.86
c_{22} (GPa)	23.6	139.0	14.352
c_{33} (GPa)	10.6	115.0	14.352
c_{12} (GPa)	3.98	77.8	5.1563
c_{13} (GPa)	2.19	74.3	5.1563
c_{23} (GPa)	1.92	74.3	7.1329
c_{45} (GPa)	6.43	30.6	5.6537
c_{56} (GPa)	2.15	25.6	3.6060
c_{46} (GPa)	4.40	25.5	5.6537
e_{15} (C/m^2)	-0.01	12.72	0
e_{24} (C/m^2)	-0.01	12.72	0
e_{31} (C/m^2)	-0.13	-5.20	0
e_{32} (C/m^2)	-0.14	-5.20	0
e_{33} (C/m^2)	-0.28	15.08	0
v_{11}/v_0	12.50	1475	3.5
v_{22}/v_0	11.98	1475	3.0
v_{33}/v_0	11.98	1300	3.0

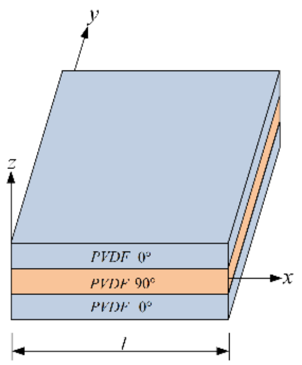

Fig. 2 Three layered piezoelectric plate model

with a consistent set of units. Properties of three different piezoelectric materials are listed in Table 1, in which v_0 represents the vacuum dielectric constant and is set as v_0=8.58×10^{-12} (F/m). To facilitate the analysis, the same unit mass density is employed for all three materials in the following dynamic examples.

5.1 Static analysis

The following four numerical exercises will explore the variations of mechanical and electric fields in laminated piezoelectric plates. Plates are subjected to the sinusoidal pressure in the form of $p(x,y)=p_0\sin(\pi x/l)\sin(\pi y/b)$ with the amplitude $p_0=1N/m^2$ on the top plane. It is essential to point out that the solutions at specific in-plane locations are presented in the following tables. These specific locations are (l/2, b/2) for u_z, Φ, σ_{zz}, σ_{xx}, σ_{yy} and D_z; (0, b/2) for u_x, τ_{xz} and D_x; (l/2, 0) for u_y, τ_{yz} and D_y; (0, 0) for τ_{xy}.

5.1.1 Three-layer cross-ply (0°/90°/0°) plate

In order to validate the accuracy and effectiveness of the proposed approach for laminated piezoelectric composite plates, exact solutions provided by Moleiro *et al*. (2014) of

Table 2 Variations of the elastic displacements through the thickness with t/l=0.1

z/t	u_x×10^{12}				u_z×10^{11}			
	2nd order	4th order	6th order	Exact	2nd order	4th order	6th order	Exact
1/2	-9.4643	-6.9272	-6.9498	-6.9373	8.0012	7.0642	7.0776	7.0691
1/3	-4.8822	-3.7091	-3.7101	-3.7051	7.9994	7.0638	7.0774	7.0690
1/6	-1.2640	-1.1000	-1.0912	-1.0897	7.9935	7.0587	7.0725	7.0640
1/6	-1.2640	-1.1000	-1.0912	-1.0897	7.9935	7.0587	7.0725	7.0640
0	0.0307	0.0265	0.0266	0.0265	7.9859	7.0515	7.0652	7.0568
-1/6	1.3172	1.1466	1.1379	1.1364	7.9778	7.0430	7.0567	7.0483
-1/6	1.3172	1.1466	1.1379	1.1364	7.9778	7.0430	7.0567	7.0483
-1/3	4.9187	3.7426	3.7436	3.7386	7.9680	7.0324	7.0460	7.0375
-1/2	9.4753	6.9407	6.9631	6.9505	7.9542	7.0171	7.0305	7.0220

three layered symmetric square plate with different thickness-span ratios are selected as benchmark examples. The piezoelectric plate consists of three cross-ply laminae (0°/90°/0°) with the material PVDF, as illustrated in Fig. 2. Fig. 3 displays that the plate is discretized with only one spectral element. Meanwhile, the elements with the second, fourth and sixth orders are utilized to investigate the structural responses of the layered piezoelectric plates. The corresponding material properties are listed in Table 1. Three thickness-span ratios t/l=0.01, 0.1 and 0.25 are under discussion in this example. The total thickness of the piezoelectric plate is set as t=0.01m and the thicknesses of the three laminae are equal. The simply supported boundary condition is prescribed at all four side faces: u_z=u_x=0 at y=0 and y=b, u_z=u_y=0 at x=0 and x=l. Zero electric potential on both the top and bottom planes are also applied. The elastic displacements, electric potential, electric displacements and stresses under the sinusoidal transverse loadings for various thickness-span ratios are listed in Tables 2-15. To conduct the convergence analysis of the present approach, the deformable behaviors of the three layered plate with the thickness-span ratio t/l=0.1 are cited as an example, as depicted in Tables 2-9. From Tables 2-15, it is clear that the through-thickness mechanical and electric quantities obtained by SBFEM show high agreement with the exact solutions from Moleiro *et al*. (2014), which confirms the accuracy and effectiveness of the proposed method to analyze the static bending behaviors of laminated piezoelectric plates. Moreover, it is necessary to indicate that increasing the element orders results in the convergent solutions calculated by the SBFEM and PIA to the exact solutions. It is believed that further refinement should lead to better results. At the same time, it is evident that only the variable D_z gets the maximum amplitude when the thickness-span ratio of the plate is t/l=0.25. However, the largest magnitudes of other mechanical and electrical variables are obtained in the thin piezoelectric plate. When the plate is thin, the deflections along the transverse direction are almost constants. With the increase of the thickness-span ratios, through-thickness distributions of the elastic transverse displacements tend to monotonically decrease.

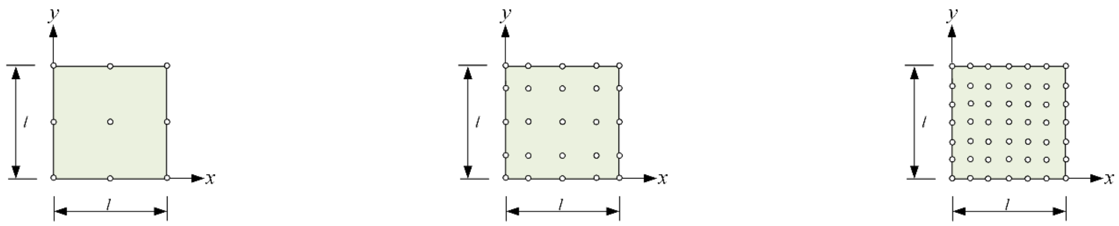

(a) The second order (b) The fourth order (c) the sixth order

Fig. 3 The plate is meshed with one spectral element of different orders

Table 3 Variations of the electric potential through the thickness with t/l=0.1

z/t	$\Phi\times10^3$			
	2nd order	4th order	6th order	Exact
1/2	0.0000	0.000	0.0000	0.0000
1/3	0.6071	0.6525	0.6606	0.6602
1/6	0.9573	1.0297	1.0426	1.0420
1/6	0.9573	1.0297	1.0426	1.0420
0	1.0598	1.1411	1.1555	1.1548
-1/6	0.9567	1.0290	1.0419	1.0413
-1/6	0.9567	1.0290	1.0419	1.0413
-1/3	0.6064	0.6515	0.6597	0.6593
-1/2	0.0000	0.0000	0.0000	0.0000

Table 4 Variations of the electric displacement D_z through the thickness with t/l=0.1

z/t	$D_z\times10^{11}$			
	2nd order	4th order	6th order	Exact
1/2	-1.5312	-1.5443	-1.5506	-1.5499
1/3	-1.5008	-1.5112	-1.5166	-1.5161
1/6	-1.4280	-1.4321	-1.4352	-1.4350
1/6	-1.4280	-1.4321	-1.4352	-1.4350
0	-1.3033	-1.2999	-1.2997	-1.2997
-1/6	-1.1785	-1.1676	-1.1641	-1.1644
-1/6	-1.1785	-1.1676	-1.1641	-1.1644
-1/3	-1.1060	-1.0888	-1.0830	-1.0835
-1/2	-1.0756	-1.0557	-1.0491	-1.0498

Table 5 Variations of the electric displacement D_x through the thickness with t/l=0.1

z/t	$D_x\times10^{11}$			
	2nd order	4th order	6th order	Exact
1/2	0.0000	0.0000	0.0000	0.0000
1/3	-1.0838	-0.7294	-0.7367	-0.7416
1/6	-1.5949	-1.1027	-1.0976	-1.1102
1/6	-2.8030	-1.8575	-1.8700	-1.8778
0	-2.8797	-1.9236	-1.9317	-1.9423
-1/6	-2.8064	-1.8600	-1.8725	-1.8804
-1/6	-1.5964	-1.1038	-1.0987	-1.1113
-1/3	-1.0832	-0.7291	-0.7363	-0.7412
-1/2	0.0000	0.0000	0.0000	0.0000

Table 6 Variations of the normal stress σ_{zz} through the thickness with t/l=0.1

z/t	$\sigma_{zz}\times10$			
	2nd order	4th order	6th order	Exact
1/2	10.0000	10.0000	10.0000	10.0000
1/3	9.2045	9.2045	9.2106	9.2587
1/6	7.3679	7.3631	7.3702	7.4071
1/6	7.3679	7.3631	7.3702	7.4071
0	4.9964	4.9958	4.9959	5.0000
-1/6	2.6225	2.6303	2.6234	2.5929
-1/6	2.6225	2.6303	2.6234	2.5929
-1/3	0.7934	0.7930	0.7871	0.7413
-1/2	0.0000	0.0000	0.0000	0.0000

Table 7 Variations of the normal stress σ_{xx} through the thickness with t/l=0.1

z/t	σ_{xx}			
	2nd order	4th order	6th order	Exact
1/2	46.2166	52.2397	53.1516	53.127
1/3	24.0597	28.0564	28.6059	28.584
1/6	6.4939	8.4534	8.6694	8.6559
1/6	1.0588	1.2765	1.3036	1.3021
0	0.0734	0.0677	0.0673	0.0673
-1/6	-0.9080	-1.1363	-1.1640	-1.1626
-1/6	-6.5455	-8.5967	-8.8184	-8.8049
-1/3	-24.0314	-28.1017	-28.6556	-28.633
-1/2	-46.0654	-52.1338	-53.0484	-53.023

Table 8 Variations of the shear stress τ_{xz} through the thickness with t/l=0.1

z/t	τ_{xz}			
	2nd order	4th order	6th order	Exact
1/2	0.0000	0.0000	0.0000	0.0000
1/3	3.5865	2.1864	2.2720	2.2528
1/6	5.1532	3.2373	3.3076	3.2905
1/6	5.1532	3.2373	3.3076	3.2905
0	5.2246	3.2968	3.3651	3.3483
-1/6	5.1611	3.2433	3.3136	3.2965
-1/6	5.1611	3.2433	3.3136	3.2965
-1/3	3.5854	2.1864	2.2715	2.2524
-1/2	0.0000	0.0000	0.0000	0.0000

Table 9 Variations of the shear stress τ_{xy} through the thickness with t/l=0.1

z/t	$\tau_{xy}\times10$			
	2nd order	4th order	6th order	Exact
1/2	-60.7478	-33.7171	-34.6571	-34.013
1/3	-36.0482	-20.2540	-20.9173	-20.423
1/6	-15.0036	-8.6170	-8.9120	-8.6860
1/6	-15.0036	-8.6170	-8.9120	-8.6860
0	0.1600	0.1096	0.1158	0.1118
-1/6	15.2975	8.8204	9.1270	8.8934
-1/6	15.2975	8.8204	9.1270	8.8934
-1/3	36.2851	20.4220	21.0964	20.594
-1/2	60.8613	33.8100	34.7593	34.108

Table 10 Distributions of the displacements and electric potential along the thickness with t/l=0.01

z/t	$u_x\times10^9$		$u_z\times10^7$		$\Phi\times10^2$	
	Exact	SBFEM	Exact	SBFEM	Exact	SBFEM
1/2	-6.5871	-6.5871	4.2221	4.2220	0.0000	0.0000
1/3	-4.3811	-4.3810	4.2222	4.2221	4.1299	4.1300
1/6	-2.1819	-2.1818	4.2223	4.2222	6.6062	6.6064
1/6	-2.1819	-2.1818	4.2223	4.2222	6.6062	6.6064
0	0.0002	0.0002	4.2223	4.2222	7.4300	7.4302
-1/6	2.1822	2.1822	4.2223	4.2222	6.6062	6.6065
-1/6	2.1822	2.1822	4.2223	4.2222	6.6062	6.6065
-1/3	4.3814	4.3814	4.2222	4.2221	4.1299	4.1300
-1/2	6.5875	6.5874	4.2221	4.2220	0.0000	0.0000

Table 11 Distributions of electric displacements and the shear stress τ_{xz} along the thickness with t/l=0.01

z/t	$D_z\times10^{11}$		$D_x\times10^{10}$		τ_{xz}	
	Exact	SBFEM	Exact	SBFEM	Exact	SBFEM
1/2	-1.5217	-1.5217	0.0000	0.0000	0.0000	0.0000
1/3	-1.4946	-1.4946	-0.6647	-0.6648	22.926	22.9310
1/6	-1.4269	-1.4269	-1.0626	-1.0628	36.645	36.6530
1/6	-1.4269	-1.4269	-1.9247	-1.9250	36.645	36.6530
0	-1.3005	-1.3005	-1.9855	-1.9859	37.363	37.3702
-1/6	-1.1740	-1.1740	-1.9247	-1.9251	36.646	36.6536
-1/6	-1.1740	-1.1740	-1.0626	-1.0628	36.646	36.6536
-1/3	-1.1063	-1.1063	-0.6647	-0.6648	22.926	22.9314
-1/2	-1.0792	-1.0792	0.0000	0.0000	0.0000	0.0000

Table 12 Distributions of normal and shear stresses along the thickness with t/l=0.01

z/t	$\sigma_{zz}\times10$		σ_{xx}		τ_{xy}	
	Exact	SBFEM	Exact	SBFEM	Exact	SBFEM
1/2	10.0000	10.0000	4992.8	4992.8658	-266.86	-266.8676
1/3	9.2587	9.2587	3320.8	3320.8708	-177.67	-177.6737
1/6	7.4071	7.4071	1654.0	1654.0190	-88.660	-88.6629
1/6	7.4071	7.4071	182.24	185.2475	-88.660	-88.6629
0	5.0000	5.0000	0.0747	0.0747	0.0090	0.0090
-1/6	2.5929	2.5929	-185.10	-185.0980	88.678	88.6809
-1/6	2.5929	2.5929	-1654.0	-1654.0678	88.678	88.6809
-1/3	0.7413	0.7413	-3320.9	-3320.9185	177.69	177.6917
-1/2	0.0000	0.0000	-4992.8	-4992.9120	266.88	266.8856

Table 13 Through-thickness variations of elastic displacements and the electric potential with t/l=0.25

z/t	$u_x\times10^{13}$		$u_z\times10^{12}$		$\Phi\times10^4$	
	Exact	SBFEM	Exact	SBFEM	Exact	SBFEM
1/2	-5.7283	-5.7375	5.0933	5.1093	0.0000	0.0000
1/3	-1.2418	-1.2525	4.9786	4.9943	2.5141	2.5201
1/6	1.4199	1.4150	4.8663	4.8819	3.8883	3.8979
1/6	1.4199	1.4150	4.8663	4.8819	3.8883	3.8979
0	0.2516	0.2514	4.7740	4.7897	4.2520	4.2629
-1/6	-1.0419	-1.0372	4.7103	4.7260	3.8405	3.8501
-1/6	-1.0419	-1.0372	4.7103	4.7260	3.8405	3.8501
-1/3	1.3862	1.3969	4.6666	4.6824	2.4553	2.4613
-1/2	5.4625	5.4737	4.6257	4.6418	0.0000	0.0000

Table 14 Through-thickness variations of electric displacements and the shear stress τ_{xz} with t/l=0.25

z/t	$D_z\times10^{11}$		$D_x\times10^{12}$		$\tau_{xz}\times10$	
	Exact	SBFEM	Exact	SBFEM	Exact	SBFEM
1/2	-1.6473	-1.6486	0.0000	0.0000	0.0000	0.0000
1/3	-1.5895	-1.5899	-4.2728	-4.1645	9.1824	9.0198
1/6	-1.4608	-1.4608	-5.5659	-5.4287	9.6155	9.5345
1/6	-1.4608	-1.4608	-7.7130	-7.5615	9.6155	9.5345
0	-1.2875	-1.2874	-8.0344	-7.8734	9.6547	9.5889
-1/6	-1.1152	-1.1151	-7.7042	-7.5538	9.6822	9.6039
-1/6	-1.1152	-1.1151	-5.5395	-5.4029	9.6822	9.6039
-1/3	-0.9903	-0.9898	-4.1414	-4.0369	8.8293	8.6804
-1/2	-0.9349	-0.9339	0.0000	0.0000	0.0000	0.0000

Table 15 Through-thickness variations of normal and shear stresses with t/l=0.25

z/t	$\sigma_{zz}\times10$		σ_{xx}		$\tau_{xy}\times10$	
	Exact	SBFEM	Exact	SBFEM	Exact	SBFEM
1/2	10.0000	10.0000	11.236	11.2770	-8.7963	-8.8454
1/3	9.0349	9.0314	2.6940	2.7124	-3.9107	-3.9780
1/6	7.1771	7.1764	-2.4042	-2.3906	-0.9642	-0.9878
1/6	7.1771	7.1764	-0.0324	-0.0306	-0.9642	-0.9878
0	4.9296	4.9296	0.0392	0.0391	0.1897	-0.1897
-1/6	2.7041	2.7048	0.1349	0.1330	1.2667	1.2899
-1/6	2.7041	2.7048	1.8960	1.8828	1.2667	1.2899
-1/3	0.9128	0.9162	-2.7631	-2.7823	4.0644	4.1322
-1/2	0.0000	0.0000	-10.526	-10.5707	8.5379	8.5947

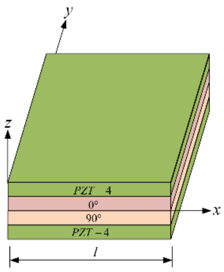

Fig. 4 Four layered (PZT-4/0°/90°/PZT-4) piezoelectric square plate

Table 16 Cross-thickness variations of displacements and electric potential with t/l=0.25

z/t	u_y×10^{12}			Φ×10			
	Exact	SBFEM	RMVT	Exact	SBFEM	RMVT	2D
1/2	-47.549	-47.5880	-45.893	0.0000	0.0000	0.0000	0.0000
9/20	-35.424	-35.3995	-33.891	0.0358	0.0353	0.0340	0.0440
2/5	-23.732	-23.8238	-22.225	0.0598	0.0599	0.0575	0.0770
2/5	-23.732	-23.8238	-22.225	0.0598	0.0599	0.0575	0.0770
1/5	0.1413	0.1300	0.1555	0.0589	0.0590	0.0567	0.0720
0	20.392	20.1685	17.260	0.0611	0.0612	0.0590	0.0700
0	20.392	20.1685	17.260	0.0611	0.0612	0.0590	0.0700
-1/5	29.110	29.1173	27.448	0.0665	0.0667	0.0645	0.0720
-2/5	39.309	39.3192	38.208	0.0756	0.0758	0.0734	0.0770
-2/5	39.309	39.3192	38.208	0.0756	0.0758	0.0734	0.0770
-9/20	49.772	50.0046	48.979	0.0425	0.0426	0.0415	0.0440
-1/2	60.678	61.0341	60.118	0.0000	0.0000	0.0000	0.0000

Table 17 Cross-thickness variations of the electric displacement and stress with t/l=0.25

z/t	D_z×10^{13}			σ_{yy}			
	Exact	SBFEM	RMVT	Exact	SBFEM	RMVT	2D
1/2	160.58	164.7009	147.89	6.5643	6.5698	6.2798	6.3538
9/20	117.23	119.9839	118.20	5.0855	5.0855	4.8373	5.2403
2/5	-0.3382	-0.3382	-0.311	3.6408	3.6457	3.4547	3.8602
2/5	-0.3382	-0.3382	-0.311	2.8855	2.8807	3.8732	2.9312
1/5	0.0813	0.0817	0.099	0.2879	0.2892	0.3008	0.2803
0	0.5052	0.5063	0.505	-1.9266	-1.9085	-2.4166	-1.9801
0	0.5052	0.5063	0.505	0.0991	0.1002	0.0522	-0.1247
-1/5	0.9563	0.9558	0.953	-0.1280	-0.1278	-0.2168	-0.2242
-2/5	1.4587	1.4552	1.433	-0.3616	-0.3626	-0.5260	-0.3685
-2/5	1.4587	1.4552	1.433	-4.2348	-4.2403	-4.0013	-4.3178
-9/20	-103.66	-106.3463	-103.84	-5.5337	-5.5496	-5.2799	-5.3752
-1/2	-142.46	-146.4667	-128.99	-6.8658	-6.8872	-6.6163	-6.8069

Table 18 Cross-thickness variations of normal and shear stresses with t/l=0.25

z/t	σ_{zz}×10		τ_{xy}×10	
	Exact	SBFEM	Exact	SBFEM
1/2	10.0000	10.0000	-2.4766	-2.5134
19/40	9.9657	9.9656	-2.1824	-2.2144
9/20	9.8682	9.8680	-1.8942	-1.9219
17/40	9.7154	9.7153	-1.6114	-1.6349
2/5	9.5151	9.5155	-1.3332	-1.3528
2/5	9.5151	9.5155	-0.2463	-0.2460
3/10	8.5199	8.5201	-0.1534	-0.1551
1/5	7.3747	7.3718	-0.0817	-0.0831
1/10	6.1686	6.1673	-0.0212	-0.0214
0	4.9831	4.9832	0.0369	0.0358
-1/10	3.8045	3.8058	0.0965	0.0995
-1/5	2.6137	2.6173	0.1529	0.1567
-3/10	1.4821	1.4883	0.2139	0.2174
-2/5	0.4868	0.4835	0.2882	0.2889
-2/5	0.4868	0.4835	1.5603	1.5890
-17/40	0.2845	0.2832	1.8105	1.8428
-9/20	0.1312	0.1309	2.0651	2.1011
-19/40	0.0340	0.0340	2.3246	2.3649
-1/2	0.0000	0.0000	2.5899	2.6347

5.1.2 Four-layer (PZT-4/0°/90°/PZT-4) composite plate

In this example, the mechanical behaviors of a four layered composite plate are investigated, as plotted in Fig. 4. The corresponding material of the inner two layer-ups is Graphite-epoxy, whose material properties are listed in Table 1. Similar with the foregoing example in Section 5.1.1, the boundary condition of the four layered piezoelectric plate is simply supported. The thickness of the coated piezoelectric and cross-ply lamina is $0.1t$ and $0.4t$ respectively. The thickness-to-length ratio t/l=0.25 is discussed, which means that a thick piezoelectric plate is studied. Through-thickness variations of the mechanical and electric variables in the four layered piezoelectric plate are delineated in Tables 16-18. From all tables, it is apparent that good agreement is achieved between the obtained results from the proposed technique and exact solutions of Heyliger (1994). The produced solutions are within less than 3.11% of error for all mechanical and electrical quantities and better than those from Carrera *et al*. (2010a) based on the Reissner mixed variational theorem (RMVT) and the 2D finite element solutions obtained by Khandelwal *et al*. (2013). In the available works of Carrera *et al*. (2010a) and Khandelwal *et al*. (2013), the distributions of mechanical and electric fields through the transverse direction are assumed to obey mathematical functions in terms of the thickness coordinate. Moreover, Carrera *et al*. (2010a) made use of the elastic displacements, electric potential, stress components and the electric displacement as the primary unknowns. Several parameters including multiple displacements and electric potential are selected as the unknown variables in the paper of Khandelwal *et al*. (2013). However, the derivation of the SBFEM governing equation is based on the three dimensional key equations of elasticity without importing any assumption on the plate kinematics. Meanwhile, only three elastic displacements and the electric potential are set as the basic unknowns, which is advantageous to improve the computational accuracy and efficiency. Throughout Tables 16-18, it can be found that the through-thickness distributions of the stresses τ_{xy} and σ_{yy} bring out the discontinuous nature at the laminae interfaces where mechanical and electrical properties abruptly change in the thickness direction. However, owing to the enforced compatibility and equilibrium boundary conditions at the interfaces of the laminated piezoelectric plate, the in-plane displacement u_y, the electric potential Φ, the normal stresses σ_{zz} and the electric displacement D_z do meet the requirement of the interlaminar continuity.

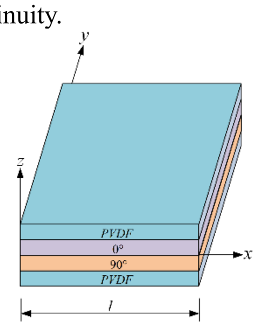

Fig. 5 Four layered (PVDF/0°/90°/PVDF) square plate model

Table 19 Variations of the displacements and electric potential along the thickness with t/l=0.01

z/t	$u_x\times10^9$ Exact	$u_x\times10^9$ SBFEM	$u_z\times10^7$ Exact	$u_z\times10^7$ SBFEM	$\Phi\times10^2$ Exact	$\Phi\times10^2$ SBFEM
1/2	-11.543	-11.5377	6.1398	6.1454	0.0000	0.0000
9/20	-10.580	-10.5744	6.1399	6.1454	1.8917	1.8933
2/5	-9.6175	-9.6126	6.1399	6.1455	3.5671	3.5701
2/5	-9.6175	-9.6126	6.1399	6.1455	3.5671	3.5701
1/5	-5.7750	-5.7712	6.1402	6.1458	3.7320	3.7353
0	-1.9334	-1.9344	6.1403	6.1459	3.8972	3.9009
0	-1.9334	-1.9344	6.1403	6.1459	3.8972	3.9009
-1/5	1.9138	1.9150	6.1401	6.1457	4.0627	4.0668
-2/5	5.7631	5.7628	6.1398	6.1453	4.2286	4.2331
-2/5	5.7631	5.7628	6.1398	6.1453	4.2286	4.2331
-9/20	6.7260	6.7253	6.1397	6.1453	2.2225	2.2248
-1/2	7.6899	7.6888	6.1397	6.1452	0.0000	0.0000

Table 20 Variations of electric displacements and the shear stress τ_{xz} along the thickness with t/l=0.01

z/t	$D_z\times10^{11}$ Exact	$D_z\times10^{11}$ SBFEM	$D_x\times10^{12}$ Exact	$D_x\times10^{12}$ SBFEM	τ_{xz} Exact	τ_{xz} SBFEM
1/2	2.1723	2.1760	0.0000	0.0000	0.0000	0.0000
9/20	2.1764	2.1800	-37.547	-37.5572	13.626	13.6424
2/5	2.1880	2.1916	-71.597	-71.6159	26.044	26.0757
2/5	2.1880	2.1916	-2.9767	-2.9788	26.044	26.0757
1/5	2.1921	2.1957	-3.1143	-3.1171	28.998	29.0151
0	2.1964	2.2001	-3.2521	-3.2557	30.075	30.0877
0	2.1964	2.2001	-3.7942	-3.7983	30.075	30.0877
-1/5	2.2010	2.2046	-3.9553	-3.9599	29.298	29.3164
-2/5	2.2057	2.2093	-4.1169	-4.1218	17.361	17.3853
-2/5	2.2057	2.2093	-54.163	-54.1933	17.361	17.3853
-9/20	2.2162	2.2198	-28.830	-28.8464	9.2845	9.2975
-1/2	2.2199	2.2235	0.0000	0.0000	0.0000	0.0000

Table 21 Variations of normal and shear stresses along the thickness with t/l=0.01

z/t	$\sigma_{zz}\times10$ Exact	$\sigma_{zz}\times10$ SBFEM	σ_{xx} Exact	σ_{xx} SBFEM	τ_{xy} Exact	τ_{xy} SBFEM
1/2	10.0000	10.0000	8692.3	8696.2207	-366.94	-367.2000
9/20	9.8798	9.8797	7962.0	7965.5076	-327.99	-328.2165
2/5	9.5336	9.5333	7232.7	7235.8921	-289.08	-289.2687
2/5	9.5336	9.5333	365.23	365.3824	-254.18	-250.2962
1/5	7.2884	7.2876	203.25	203.3206	-117.46	-115.6143
0	4.7132	4.7132	41.299	41.2844	19.226	19.0360
0	4.7132	4.7132	783.44	783.4941	19.226	19.0360
-1/5	2.2529	2.2537	-855.56	-856.2785	156.00	153.7693
-2/5	0.3518	0.3521	-2495.4	-2496.6451	292.83	288.5575
-2/5	0.3518	0.3521	-4424.3	-4427.0450	333.04	333.4876
-9/20	0.0916	0.0917	-5154.1	-5157.1935	371.98	372.4444
-1/2	0.0000	0.0000	-5884.6	-5888.0738	410.91	411.4304

Table 22 Through-thickness distributions of elastic displacements and electric potential with t/l=0.1

z/t	$u_x\times10^{12}$		$u_z\times10^{11}$		$\Phi\times10^4$	
	Exact	SBFEM	Exact	SBFEM	Exact	SBFEM
1/2	-11.005	-11.0094	7.7151	7.7195	0.0000	0.0000
9/20	-9.8676	-9.8756	7.7166	7.7210	3.0586	3.0625
2/5	-8.8696	-8.8786	7.7175	7.7218	5.8423	5.8494
2/5	-8.8696	-8.8786	7.7175	7.7218	5.8423	5.8494
1/5	-5.4703	-5.4727	7.7351	7.7388	5.4790	5.4869
0	-2.1850	-2.1737	7.7357	7.7392	5.1626	5.1712
0	-2.1850	-2.1737	7.7357	7.7392	5.1626	5.1712
-1/5	1.6168	1.6225	7.7137	7.7174	4.8904	4.8996
-2/5	5.6002	5.6012	7.6724	7.6768	4.6600	4.6697
-2/5	5.6002	5.6012	7.6724	7.6768	4.6600	4.6697
-9/20	6.6515	6.6529	7.6661	7.6707	2.4652	2.4705
-1/2	7.8004	7.7996	7.6592	7.6638	0.0000	0.0000

Table 23 Through-thickness distributions of electric displacements and the shear stress τ_{xz} with t/l=0.1

z/t	$D_z\times10^{13}$		$D_x\times10^{13}$		τ_{xz}	
	Exact	SBFEM	Exact	SBFEM	Exact	SBFEM
1/2	-6.9318	-6.9285	0.0000	0.0000	0.0000	0.0000
9/20	-6.4704	-6.4642	-40.056	-39.8268	1.2944	1.3141
2/5	-5.1500	-5.1396	-76.104	-75.8615	2.4546	2.4928
2/5	-5.1500	-5.1396	-4.8753	-4.8701	2.4546	2.4928
1/5	-4.5047	-4.4952	-4.5721	-4.5885	2.7647	2.8035
0	-3.9033	-3.8926	-4.3081	-4.3371	2.8865	2.9240
0	-3.9033	-3.8926	-5.0261	-5.0600	2.8865	2.9240
-1/5	-3.3327	-3.3234	-4.7611	-4.7996	2.8795	2.9084
-2/5	-2.7906	-2.7830	-4.5368	-4.5693	1.7394	1.7626
-2/5	-2.7906	-2.7830	-55.739	-56.3811	1.7394	1.7626
-9/20	-1.6670	-1.6626	-29.909	-30.2984	0.9388	0.9529
-1/2	-1.2712	-1.2726	0.0000	0.0000	0.0000	0.0000

Table 24 Through-thickness distributions of normal and shear stresses with t/l=0.1

z/t	$\sigma_{zz}\times10$		σ_{xx}		τ_{xy}	
	Exact	SBFEM	Exact	SBFEM	Exact	SBFEM
1/2	10.000	10.0000	83.255	83.3634	-3.7953	-3.7807
9/20	9.8836	9.8837	74.628	74.7203	-3.3247	-3.3124
2/5	9.5512	9.5524	67.039	67.1129	-2.8891	-2.8790
2/5	9.5512	9.5524	3.9285	3.9327	-2.5403	-2.5166
1/5	7.3338	7.3310	2.2947	2.2946	-1.1308	-1.1182
0	4.7586	4.7583	0.6915	0.6879	0.2371	0.2321
0	4.7586	4.7583	9.0138	8.9757	0.2371	0.2321
-1/5	2.2954	2.2964	-7.3129	-7.3363	1.6816	1.6852
-2/5	0.3625	0.3638	-24.390	-24.4033	3.1818	3.1720
-2/5	0.3625	0.3638	-43.202	-43.2242	3.6187	3.6000
-9/20	0.0949	0.0954	-51.183	-51.2185	4.0579	4.0370
-1/2	0.0000	0.0000	-59.895	-59.9490	4.5273	4.5041

Table 25 Distributions of elastic displacements and electric potential through the thickness with t/l=0.25

z/t	$u_x\times10^{13}$		$u_z\times10^{12}$		$\Phi\times10^4$	
	Exact	SBFEM	Exact	SBFEM	Exact	SBFEM
1/2	-6.1636	-6.1867	4.1492	4.1787	0.0000	0.0000
9/20	-4.8010	-4.8236	4.1158	4.1452	1.4573	1.4591
2/5	-3.8982	-3.8928	4.0812	4.1104	2.8257	2.8286
2/5	-3.8982	-3.8928	4.0812	4.1104	2.8257	2.8286
1/5	-2.4154	-2.4121	4.0000	4.0284	2.2036	2.2080
0	-1.6898	-1.6400	3.9221	3.9501	1.6998	1.6951
0	-1.6898	-1.6400	3.9221	3.9501	1.6998	1.6951
-1/5	0.5556	0.5669	3.8345	3.8630	1.2873	1.2931
-2/5	3.2144	3.2101	3.7372	3.7667	0.9439	0.9499
-2/5	3.2144	3.2101	3.7372	3.7667	0.9439	0.9499
-9/20	4.0579	4.0640	3.7240	3.7537	0.5125	0.5185
-1/2	5.2880	5.3010	3.7099	3.7397	0.0000	0.0000

Table 26 Distributions of electric displacements and the shear stress τ_{xz} through the thickness with t/l=0.25

z/t	$D_z\times10^{13}$		$D_x\times10^{13}$		$\tau_{xz}\times10$	
	Exact	SBFEM	Exact	SBFEM	Exact	SBFEM
1/2	-12.195	-12.2071	0.0000	0.0000	0.0000	0.0000
9/20	-11.414	-11.4123	-22.675	-22.5152	4.4022	4.3428
2/5	-9.1882	-9.1965	-42.551	-42.5059	7.9127	7.9214
2/5	-9.1882	-9.1965	-5.8951	-5.8795	7.9127	7.9214
1/5	-7.4106	-7.3948	-4.5972	-4.6061	9.4753	9.4678
0	-6.031	-6.0366	-3.5462	-3.5695	10.217	10.1847
0	-6.031	-6.0366	-4.1372	-4.1645	10.217	10.1847
-1/5	-4.9752	-4.9675	-3.1332	-3.1692	10.820	10.6816
-2/5	-4.1866	-4.1878	-2.2974	-2.3369	6.9496	6.8397
-2/5	-4.1866	-4.1878	-23.993	-23.8927	6.9460	6.8397
-9/20	-2.8632	-2.8774	-13.272	-13.1764	3.8792	3.8021
-1/2	-2.3863	-2.4213	0.0000	0.0000	0.0000	0.0000

Table 27 Distributions of normal and shear stresses through the thickness with t/l=0.25

z/t	$\sigma_{zz}\times10$		σ_{xx}		$\tau_{xy}\times10$	
	Exact	SBFEM	Exact	SBFEM	Exact	SBFEM
1/2	10.000	10.0000	11.949	11.9808	-7.1052	-7.0663
9/20	9.8918	9.8914	9.3611	9.3878	-5.6523	-5.6217
2/5	9.5973	9.5989	7.6326	7.5689	-4.5643	-4.5122
2/5	9.5973	9.5989	0.9113	0.9097	-3.9869	-3.9043
1/5	7.4425	7.4414	0.5847	0.5841	-1.2867	-1.2600
0	4.8594	4.8606	0.3151	0.3122	0.7711	0.7819
0	4.8594	4.8606	1.8700	1.8411	0.7711	0.7819
-1/5	2.4028	2.4034	-0.6341	-0.6365	3.3006	3.2824
-2/5	0.3940	0.3932	-3.5654	-3.5744	6.2640	6.1771
-2/5	0.3940	0.3932	-6.3010	-6.3167	7.1241	7.1389
-9/20	0.1053	0.1055	-7.9109	-7.9168	8.0687	8.0738
-1/2	0.0000	0.0000	-10.246	-10.2564	9.3495	9.3450

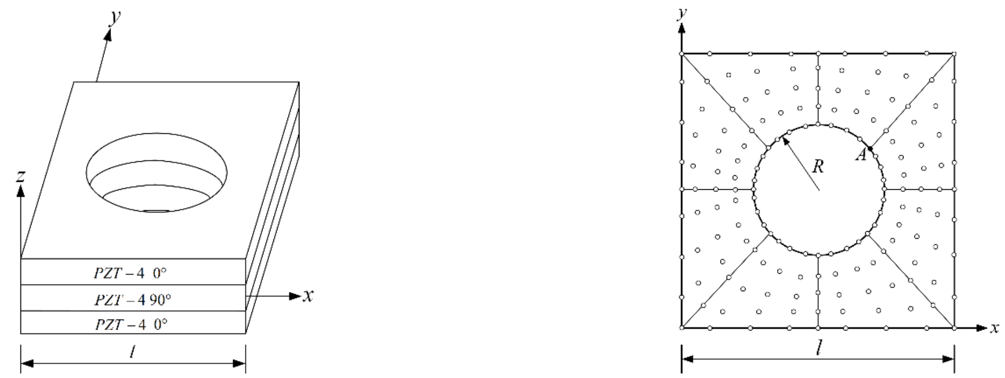

(a) The plate model (b) Meshed with eight fourth-order spectral elements

Fig. 6 Three-layer piezoelectric perforated plate

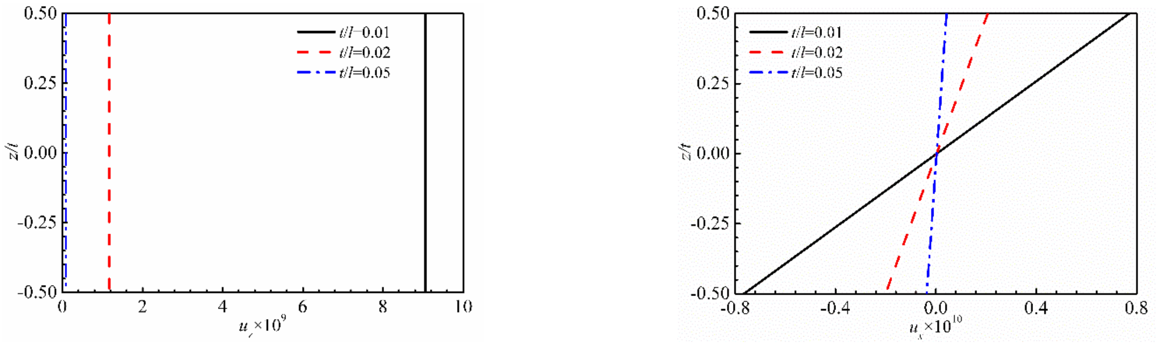

(a) u_z (b) u_x

Fig. 7 Cross-thickness distributions of the elastic displacements

5.1.3 Four-layer (PVDF/0°/90°/PVDF) composite plate

To further demonstrate the soundness of the present approach in dealing with the mechanical behaviors of a four layered piezoelectric plate, a plate using (PVDF/0°/90°/PVDF) as the make-ups is taken as an example, as illustrated in Fig. 5. The material of the middle part is Graphite-epoxy and its relevant material constants are listed in Table 1. Three different thickness-to-length ratios t/l=0.01, 0.1 and 0.25 are considered, which are corresponding to thin, moderately thick and thick plates, respectively. The entire thickness of the piezoelectric plate is t=0.01m. The thickness of the first and fourth PVDF lamina is 0.1t and the two core layers have the equal thickness 0.4t. The same simply supported boundary constraints as the foregoing examples are imposed on the four boundary edge surfaces. Tables 19-27 reveal the variations of elastic displacements, electric potential, stresses and electric displacements along the thickness direction. From Tables 19-27, it is obvious that the introduced methodology can provide excellent results when compared with the 3D exact solutions of *Moleiro et al*. (2014). The maximum difference is only 2.95% for the in-plane elastic displacement u_x in the thick plate. In Table 19, the distribution curve of the deflections through the thickness tends to a vertical straight line in the thin plate, which is consistent with the conclusion from the foregoing example. What's more, it is observed that the maxima of the shear stress τ_{xz} appear in the middle of the plate. However, magnitudes of the in-plane displacement u_x, normal stress σ_{xx} and the electric displacement D_z will peak at the upper or lower surface.

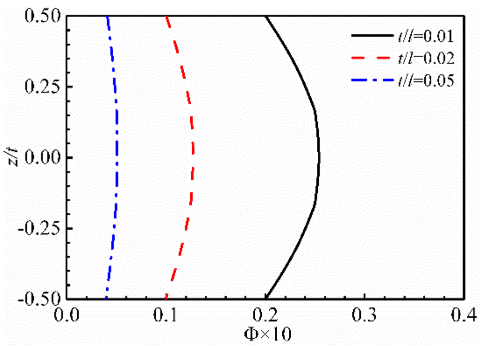

Fig. 8 Cross-thickness distributions of the electric potential

5.1.4 Three-layer square plate with a circular hole

In order to display the effectiveness of the introduced method in examining the bending problem of the laminated piezoelectric plates with more complex shapes, a three layered cross-ply square plate with a central circular hole is shown as an example, as illustrated in Fig. 6. The plate is composed of three cross ply laminae (0°/90°/0°) using the material PZT-4. The length of the square plate is l=b=1m and the radius of the inner circular hole is set as R=l/4. A wide range of thickness-to-length ratios t/l=0.01, 0.02 and 0.05 is under consideration. In the laminated composite plate, each lamina has the equal thickness. All the four side faces of the square plate are clamped, which means that

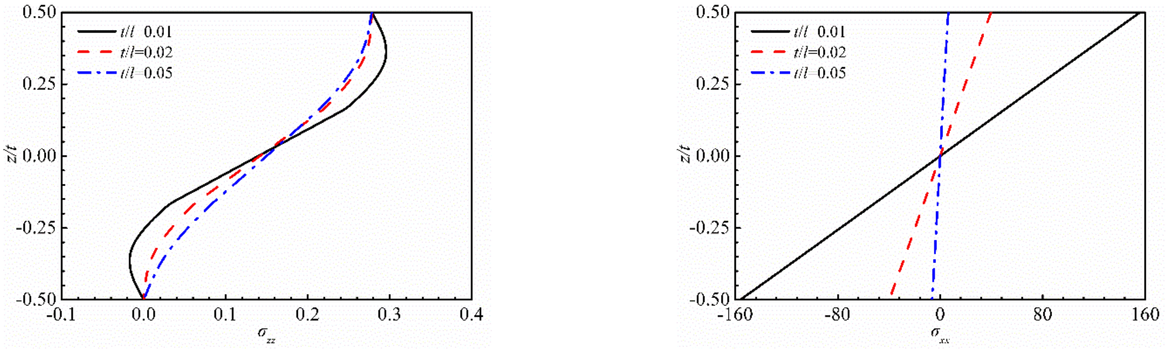

(a) σ_{zz} (b) σ_{xx}

Fig. 9 Cross-thickness distributions of the normal stresses

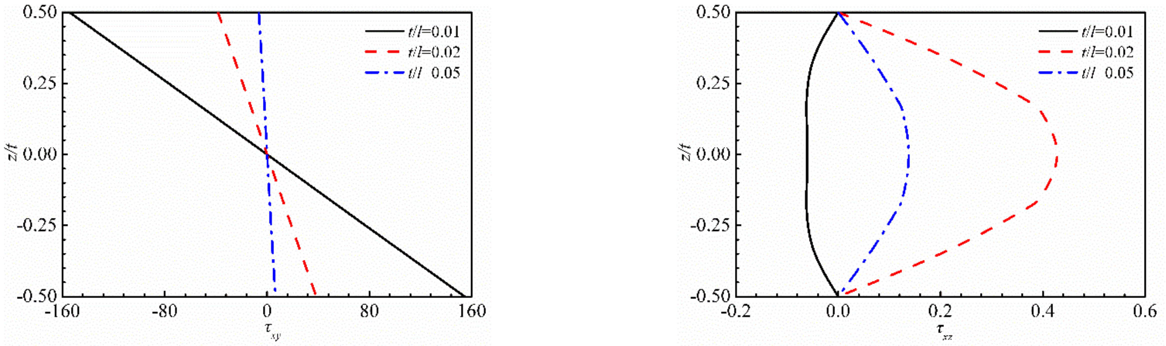

(a) τ_{xy} (b) τ_{xz}

Fig. 10 Cross-thickness distributions of the shear stresses

$u_z=u_x=u_y=\Phi=0$ at $x=0$, $x=l$, $y=0$ and $y=b$. However, the inner circular boundary is completely free. Different from the above examples, this section pays attention to the variations of mechanical and electrical variables at the point $A\left(\frac{\sqrt{2}R}{2}, \frac{\sqrt{2}R}{2}\right)$. Figs. 7-11 exhibit the distributions of elastic displacements, electric potential, stresses and electric displacements along the thickness of the multilayered piezoelectric plate with a circular hole. From Fig. 7, it is obvious that the magnitudes of the elastic displacements in z and x directions decrease with the increase of the thickness-to-length ratios, which means that increasing the thickness-to-length ratios may increase the stiffness of the piezoelectric plates and thus leads to lower displacements. The similar phenomenon can also be found for the electric potential in Fig. 8. But the maxima of the electric potential appear at the middle surface of the plate. As to the normal stresses σ_{xx} in Fig. 9, it can be found that σ_{xx} are tensile in the first laminate, compressive in the third layer and reach zero at the mid-plane of the second layer. Moreover, it is noticed that the normal stress σ_{xx} and shear stress τ_{xy} vary linearly along the thickness. However, the variations of the normal stress σ_{zz}, shear stress τ_{xz}, electric displacements D_z and D_x present the pattern of curve changes. Regarding the shear stress τ_{xz} and electric displacement D_x, it is observed that the variation curves of the aspect ratio t/l=0.01 show greatly different trends compared with those of other aspect ratios. A conclusion can be drawn that the thickness-to-length ratio significantly influences the distributions of the mechanical and electric quantities.

5.2 Free vibration analysis

Due to the fact that the dynamic responses of laminated piezoelectric composite plates are vital for design and application in many practical applications, it is important and essential to investigate the transverse vibration characteristics. In this section, three examples are provided to demonstrate the effectiveness of the proposed technique to evaluate the vibration frequencies. The three and five layered square and rhombic piezoelectric plates are under consideration. The natural frequencies in these three examples are normalized as $\bar{\omega}=\frac{\omega}{100}$, in which ω is the circular vibration parameters.

5.2.1 Three layered symmetric plate

This example carries out the free vibration analysis of a three layered simply supported symmetric piezoelectric plate composed of the transversely isotropic materials PZT-4 and PVDF. The stacking sequences of the laminated plate are PZT-4/PVDF/PZT-4 and PVDF/PZT-4/PVDF with the material properties listed in Table 1. The total thickness of the layered piezoelectric plate is t=0.01m. The thickness of the top and bottom layer is 0.25t, as shown in Fig. 12. The free vibration responses of the piezoelectric plates with two thickness-to-length ratios t/l=0.02 and 0.25 are considered. The thickness-to-length ratios t/l=0.02 and 0.25 are corresponding to thin and thick plates, respectively. Two different boundary conditions of Case 1: zero electric potential Φ on both the top and bottom planes and Case 2:

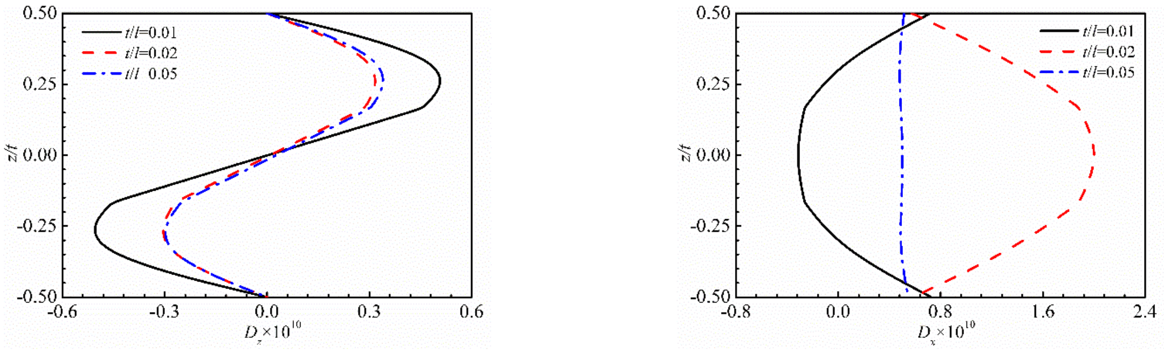

(a) D_z (b) D_x

Fig. 11 Cross-thickness distributions of the electric displacements

(a) PZT-4/PVDF/PZT-4 (b) PVDF/PZT-4/PVDF

Fig. 12 Three layered piezoelectric plate

zero electric displacement D_z on the upper and lower surfaces are studied. The vibration frequencies of the simply supported piezoelectric plate are presented in Tables 28-35. The exact eignsolutions from Heyliger and Saravanos (1995b) and the 2D closed form results obtained by Benjeddou and Deü (2002a) are also provided in these tables for comparison. Investigations of the normalized natural frequencies in Tables 28-35 reveal that the proposed approach is able to predict highly accurate results which are in very good matching with those of Heyliger and Saravanos (1995b) under different stacking sequences, boundary conditions and thickness-to-length ratios for both thin and thick piezoelectric plates. Additionally, it should be noted that with the increase of the spectral element orders the transverse vibration parameters acquired by the SBFEM and PIA converge to the exact solutions. Therefore, the accuracy of the present semi-analytical technique in determining natural frequencies of laminated piezoelectric plates can be confirmed. Comparing with the 2D solutions form Benjeddou and Deü (2002a), the non-dimensional eigenvalues evaluated by the introduced method are closer to the exact solutions. Benjeddou and Deü (2002a) adopted the first order shear deformation plate theory to model a linearly-varied displacement field along the thickness in a layer and assumed the through-thickness electric potential according to a quadratic function of z-coordinates. However, the displacement components and electric potential through the transverse direction can be analytically formulated and no assumptions have been added in the SBFEM. From Tables 28-35, it can be seen that the great differences of vibration frequencies under the two types of stacking sequences have happened when the boundary condition and thickness-to-length ratio are same. In other words, the stacking sequences play an important role in estimating the eigenvalues of laminated piezoelectric plates.

Table 28 Natural frequencies of the PZT-4/PVDF/PZT-4 plate with t/l=0.02 and Case 1

Mode	2^{nd} order	3^{rd} order	4^{th} order	Exact	2D
1	768.1424	726.5187	725.2111	725.219	725.230
2	16450.2730	16430.9891	16430.1786	16430.2	16436.9
3	28068.9538	28530.0591	28532.5264	28535.7	28540.4
4	160389.2075	159801.5404	159607.0203	159732	161063.6
5	226167.7985	226515.0906	226193.0474	226218	228455.9
6	346648.4124	350738.9276	352725.9532	353386	

Table 29 Natural frequencies of the PZT-4/PVDF/PZT-4 plate with t/l=0.02 and Case 2

Mode	2^{nd} order	3^{rd} order	4^{th} order	Exact	2D
1	768.2215	726.5450	725.2331	725.241	725.252
2	16459.1845	16439.6399	16438.8257	16438.8	16445.6
3	28960.7796	28549.3683	28551.8806	28555.1	28559.9
4	160566.6366	159905.5123	159963.8162	159865	161204.3
5	226763.0985	226777.3730	226322.3173	226643	228903.6
6	355354.3340	355350.5560	362188.8956	363810	

Table 30 Vibration frequencies of the PVDF/PZT-4/PVDF plate with t/l=0.02 and Case 1

Mode	2nd order	3rd order	4th order	Exact	2D
1	684.3101	635.1891	633.4267	633.417	633.666
2	16451.2218	16431.9303	16431.1200	16431.1	16432.5
3	28947.8667	28529.5948	28532.0538	28535.2	28537.6
4	265099.4804	268119.6752	268044.0103	268118	292031.9
5	351025.4710	351617.9737	353090.1385	353079	379316.5
6	361063.2252	363760.0350	371636.4879	369396	

Table 31 Vibration frequencies of the PVDF/PZT-4/PVDF plate with t/l=0.02 and Case 2

Mode	2nd order	3rd order	4th order	Exact	2D
1	684.4257	635.2611	633.4963	633.487	633.735
2	16461.2645	16441.7115	16440.8977	16440.9	16442.3
3	28084.6838	28549.6534	28553.1530	28555.3	28557.7
4	268155.8460	271115.5912	271133.3232	271222	295866.2
5	362560.0676	362085.1930	362572.6829	362248	390810.4
6	367871.4845	369412.2875	368663.8606	369397	

Table 32 Eigenvalues of the PZT-4/PVDF/PZT-4 plate with t/l=0.25 with Case 1

Mode	2nd order	3rd order	4th order	Exact	2D
1	58581.7699	58114.6111	58045.1001	58248.7	58339.5
2	193033.9026	192180.7132	192622.9051	192408	204629.8
3	268054.0397	268976.8833	269192.8820	271757	275428.9
4	331423.5820	330629.6936	329097.9333	329584	355778.2
5	366304.5435	362884.9588	363549.4557	363048	413006.4
6	401421.5918	404941.6802	406183.3792	406665	

Table 33 Eigenvalues of the PZT-4/PVDF/PZT-4 plate with t/l=0.25 with Case 2

Mode	2nd order	3rd order	4th order	Exact	2D
1	58706.5146	58217.9831	58146.1878	58354	58445.4
2	192671.8861	192209.8394	192062.1027	192436	204650
3	272627.4168	273962.2880	271686.8661	271758	275429.3
4	331433.0502	330806.8748	329135.8457	329593	356148.2
5	366304.5445	363161.4604	368200.0755	364072	414334.3
6	403386.9150	409271.3724	406307.8570	407771	

Table 34 Eigenvalues of the PVDF/PZT-4/PVDF plate with t/l=0.25 with Case 1

Mode	2nd order	3rd order	4th order	Exact	2D
1	72756.1580	71895.8442	71796.6695	72174.4	73969.5
2	194379.3950	194522.7834	194944.3910	194760	197165
3	303820.0080	306140.7494	306236.8137	306209	329399.5
4	339915.9597	338682.4932	338936.0431	337107	345026.8
5	423722.3171	424618.9436	424456.2620	424602	459653.3
6	528137.8067	529499.8391	529143.1088	529129	

Table 35 Eigenvalues of the PVDF/PZT-4/PVDF plate with t/l=0.25 with Case 2

Mode	2nd order	3rd order	4th order	Exact	2D
1	72776.2770	71912.4058	71813.090	72191.5	74006
2	195066.1362	194643.0069	194500.1067	194881	197279.6
3	303924.0051	306305.0203	306320.7014	306539	329861.6
4	339966.8598	336268.4825	338964.9135	337196	345226
5	424618.9444	424741.3515	425816.6742	424664	459693.3
6	530193.0248	530903.0926	529483.7342	529543	

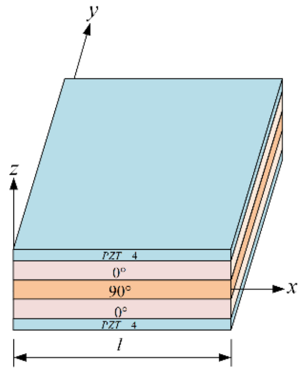

Fig. 13 Five layered hybrid plate model

5.2.2 Five layered hybrid composite plate

To further demonstrate the effectiveness and feasibility of the proposed method in calculating the frequencies of laminated piezoelectric plate, a five layered hybrid composite plate is shown as an example, as exhibited in Fig. 13. The hybrid piezoelectric plate is comprised by the laminae of PZT-4/0°/90°/0°/PZT-4, in which the material of the cross-ply layer is Graphite-epoxy. The material constants of PZT-4 and Graphite-epoxy are listed in Table 1. Similar with the foregoing section, two different aspect ratios t/l=0.02 and 0.25 are under consideration, in which t and l represent the whole thickness and length of the square plate. The thickness of each PZT-4 lamina on the top and bottom surfaces is $0.1t$ and the inner three laminae have equal thickness $8/30t$. The same boundary condition as that used in Section 5.2.1 are applied. Eigensolutions of the five layered piezoelectric composite plate are released in Tables 36-37. From these tables, it is apparent that the results obtained by the developed methodology are in excellent agreement with the exact solutions from Heyliger and Saravanos (1995) and better than the 2D solutions gained by Benjeddou and Deü (2002a) for all aspect ratios and boundary conditions. Regardless of the thin and thick piezoelectric plates, the errors between the present results and exact solutions are all less than 1%, which proves the accuracy of the proposed method once again. When the same boundary conditions are utilized on the piezoelectric plate, the vibration frequencies with the aspect ratio t/l=0.02 are smaller than those with t/l=0.25. Meanwhile, the mode frequencies of the Case 1 and Case 2 are slightly different. It is believed that the aspect ratio as a key factor has outstanding influences on the free vibration responses of laminated hybrid piezoelectric composite plates.

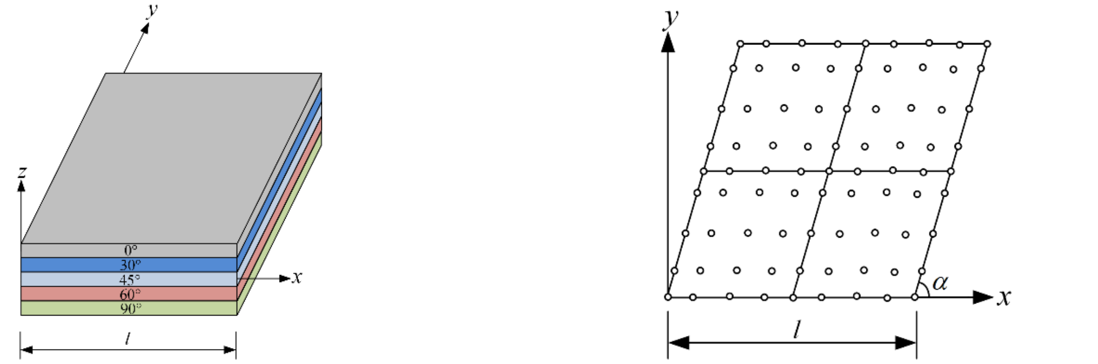

(a) The rhombic plate model (b) Meshed with fourth order spectral elements

Fig. 14 Five-layer composite piezoelectric plate

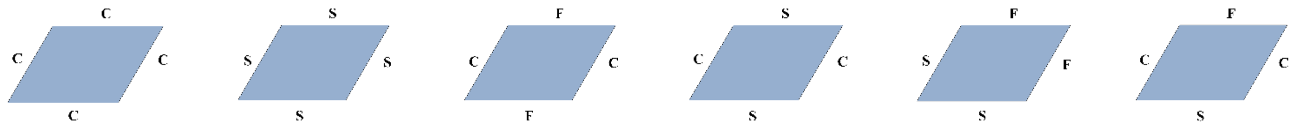

(a) CCCC (b) SSSS (c) FCFC (d) SCSC (e) SSFF (f) SCFC

Fig. 15 The six types of boundary conditions for the rhombic plate

Table 36 Mode frequencies of the five layered hybrid plate with t/l=0.02

Mode	Case 1			Case 2		
	Exact	SBFEM	2D	Exact	SBFEM	2D
1	618.118	618.1059	618.435	618.12	618.1081	618.437
2	15681.6	15681.3704	15684	15681	15681.3097	15684
3	21492.8	21492.4224	21499.4	21493	21493.1419	21499.6
4	209704	209746.5343	214834	209707	209746.5343	214865.6
5	210522	210566.1593		210573	210585.3105	
6	378104	378204.6020		378105	378017.3330	

Table 37 Eigensolutions of the five layered hybrid plate with t/l=0.25

Mode	Case 1			Case 2		
	Exact	SBFEM	2D	Exact	SBFEM	2D
1	57074.5	56981.2327	58216.1	57089.3	56995.8915	58231
2	191301	191174.0700	196017.7	191304	191176.8511	196019.9
3	250769	251046.6369	268650	250770	250271.8062	268650.2
4	274941	273698.7633	283754.1	274941	273912.1467	283754.1
5	362492	362466.0009		362522	361802.8699	
6	381036	381117.9701		381049	381131.0903	

Table 38 Eigensolutions of the five-layer rhombic plate with α=15°

	CCCC	SSSS	FCFC	SCSC	SSFF	SCFC
1	4066.8900	3206.6941	1731.8236	3227.7207	83.9103	1761.6093
2	5786.8816	4390.1308	1787.2733	4425.1927	377.7869	3105.4758
3	8116.2557	6349.0242	3052.1791	6401.0033	787.8980	4072.1538
4	9683.6105	8312.5389	3774.8619	8346.0654	948.6738	5398.6100
5	11108.5146	9100.4150	4898.0658	9248.6732	1049.6613	6811.0465
6	13096.4869	11394.3917	6031.8603	11432.7184	2055.3737	7656.8325

Table 39 Eigenvalues of the five-layer rhombic plate with α=30°

	CCCC	SSSS	FCFC	SCSC	SSFF	SCFC
1	1220.1741	907.7389	568.9829	924.0585	68.7098	593.1793
2	1879.0026	1382.7243	620.4998	1410.2592	274.9775	965.5458
3	2817.0902	2125.9105	1014.3595	2163.3160	497.0205	1431.5244
4	3048.7471	2481.1295	1407.3079	2518.4455	608.8749	1775.7855
5	4108.0128	3184.0898	1758.2974	3252.6420	999.0912	2346.5497
6	4415.1259	3665.0410	1894.5401	3708.2028	1095.7946	2599.3070

Table 40 Vibration frequencies of the five-layer rhombic plate with α=45°

	CCCC	SSSS	FCFC	SCSC	SSFF	SCFC
1	636.8413	461.1480	329.4893	475.2592	60.5584	348.2790
2	1047.5409	789.7239	381.4994	816.0823	225.9525	546.3823
3	1534.4277	1206.4718	619.2026	1243.0933	345.4604	881.9924
4	1587.9417	1225.8199	882.7574	1259.7124	463.6601	987.1463
5	2292.4984	1814.8409	1042.0526	1875.7964	754.0493	1379.8601
6	2324.2062	1913.9768	1049.5979	1957.7032	804.2129	1409.6630

5.2.3 Five-layer composite rhombic plate

To exhibit the versatility and applicability of the employed technique in studying the free vibration responses of multilayered angle-ply piezoelectric plates, a five layered hybrid rhombic plate (0°/30°/45°/60°/90°) constituted by the Graphite-epoxy material with different skew angles and boundary constraints is shown as an example, as displayed in Fig. 14. Fig. 15 depicts the six different kinds of boundary conditions CCCC, SSSS, FCFC, SCSC, SSFF and SCFC, in which S stands for the simply supported constraint, C represents the clamped boundary and F means the free boundary. In this section, the simply supported and clamped boundary conditions are the same as those used in

Table 41 Natural frequencies of the five-layer rhombic plate with α=60°

	CCCC	SSSS	FCFC	SCSC	SSFF	SCFC
1	444.9562	315.6181	257.5857	337.9601	54.3016	270.0494
2	795.5229	597.6456	300.0200	629.7978	199.4142	409.7683
3	1007.3163	779.6623	491.1773	836.2188	270.0046	714.9677
4	1197.2115	934.9984	706.3885	981.7527	410.7979	740.5927
5	1593.8819	1329.7819	783.5366	1375.0880	559.0693	965.2218
6	1730.4171	1384.0465	829.0902	1455.5157	651.6003	1107.7211

the foregoing examples. The geometric parameters of the plate are set as l=1m, t=0.02m. Each layer has the equal thickness. Four different skew angles α=15°, 30°, 45° and 60° are under consideration. In all situations, zero electric potentials are imposed on both the top and bottom planes. Natural frequencies of the five layered angle-ply rhombic plate under different skew angles and boundary conditions are listed in Tables 38-41. From these tables, it is clear that with the increase of skew angles, the corresponding dimensionless vibration frequencies decrease when the same boundary constraints are applied, which is owing to the detraction of the flexural stiffness with the larger skew angle. What's more, the decrease of the natural frequencies is significant when the skew angle increases from 15° to 30°. However, there is a small change of eigenvalues with the skew angle increasing from 30° to 60°. Additionally, it is found that increasing the number of the clamped edge faces correspondingly leads the increase of the natural frequencies. As expected, the multilayered CCCC piezoelectric plate produces the largest vibration frequencies over other boundary conditions, which is parallel with the former findings. When the rhombic piezoelectric plates with the same skew angle are under discussion, the distributions of dimensionless eigenvalues obey the following pattern CCCC>SCSC>SSSS>SCFC>FCFC>SSFF. It can be concluded that skew angles and boundary conditions make a great influence on the variations of eigensolutions in multilayered piezoelectric plates.

6. Conclusions

The distributions of elastic displacements, electric potential, stresses, electric displacements and transverse vibration frequencies in the laminated piezoelectric composite plates are investigated based on the SBFEM and PIA in this work. The proposed approach is applicable to multilayered piezoelectric plates with any number of laminae, various geometrical shapes, boundary constraints and thickness-to-length ratios. Only a surface perpendicular to the thickness direction is discretized into 2D elements, which helps to improve the computational efficiency. Comparing with plate theories and other numerical methods, only three translational displacements and the electric potential are set as the basic unknowns and can be formulated analytically along the transverse direction. The whole derivation of the SBFEM governing equation is built upon the three dimensional key equations of elasticity for piezoelectric materials and no assumptions on the plate kinematics have been taken, which is unlike other methods enforcing the priori assumptions on the variations of the mechanical and electric quantities. The general solution of the governing equation is in the form of a matrix exponent. To further improve the accuracy of the matrix exponent, the PIA is employed to ensure any desired accuracy of the mechanical and electrical variables. By means of the kinetic energy technique, this article constructs the global mass matrix of the multilayered piezoelectric plate for the first time based on the SBFEM.

From all tables, it is apparent that solutions of the developed methodology are in excellent agreement with the exact solutions available in the literatures, which means that the accuracy and effectiveness of the introduced semi-analytical technique can be confirmed. In the three layered plate, only the electric displacement D_z gets the maximum amplitude with the thickness-span ratio t/l=0.25. While the largest magnitudes of other mechanical and electrical variables are obtained in the thin plate. With regard to the (PZT-4/0°/90°/PZT-4) plate, it is found that the through-thickness variations of the stresses τ_{xy} and σ_{yy} bring out the discontinuous nature at the laminae interfaces. In the four layered (PVDF/0°/90°/PVDF) plate, it is observed that the maxima of the shear stress τ_{xz} appear in the middle of the plate. However, amplitudes of the in-plane displacement u_x, normal stress σ_{xx} and the electric displacement D_z will peak at the upper or lower plate surface. Regarding the three layered perforated piezoelectric plate, the thickness-to-length ratio significantly influences the distributions of the mechanical and electric fields. As to the dynamic responses, it can be seen that the great differences of vibration frequencies have happened between the two plates with the stacking sequences PZT-4/PVDF/PZT-4 and PZT-4/PVDF/PZT-4. In the plate constituted by the layer-ups PZT-4/0°/90°/0°/PZT-4, the eigensolutions of the aspect ratio t/l=0.02 are remarkably different from those of t/l=0.25. For the rhombic plate, it is found that with the increase of skew angles, the vibration frequencies decrease when the same boundary condition are applied. It can be concluded that boundary conditions, stacking sequences, thickness-to-length ratios and skew angles have significant influences on the static and dynamic responses of the laminated piezoelectric composite plates. More meaningful results will be explored in forthcoming papers.

Acknowledgments

This research is supported by Grants 2018M641168 from China Postdoctoral Science Foundation, Grants

51908022, 2015CB57800 and 51774018 from the National Natural Science Foundation of China, Grant IRT_17R06 from program for Changjiang Scholars and Innovative Research Team, Grants 19YJC630148 from the Humanity and Social Science Youth foundation of Ministry of Education of China, for which the authors are gratefully acknowledged.

References

Akhras, G., and Li, W.C. (2007), "Three-dimensional static, vibration and stability analysis of piezoelectric composite plates using a finite layer method", *Smart Mater. Struct.*, **16**(3), 561-569. http://dx.doi.org/10.1088/0964-1726/16/3/002.

Akhras, G., and Li, W.C. (2007), "Three-dimensional static, vibration and stability analysis of piezoelectric composite plates using a finite layer method", *Smart Mater. Struct.*, **16**(3), 561-569. http://dx.doi.org/10.1088/0964-1726/16/3/002.

Akhras, G., and Li, W.C. (2011), "Stability and free vibration analysis of thick piezoelectric composite plates using spline finite strip method", *Int. J. Mech. Sci.*, **53**(8), 575-584. http://dx.doi.org/10.1016/j.ijmecsci.2011.05.004.

Askari, M., Saidi, A.R., and Rezaei, A.S. (2018), "An investigation over the effect of piezoelectricity and porosity distribution on natural frequencies of porous smart plates", *J. Sandwich Struct. Mater.*. http://dx.doi.org/10.1177/1099636218791092.

Baghaee, M., Farrokhabadi, A., and Jafari-Talookolaei, R.A. (2019), "A solution method based on Lagrange multipliers and Legendre polynomial series for free vibration analysis of laminated plates sandwiched by two MFC layers", *J. Sound Vibr.*, **447**, 42-60. https://doi.org/10.1016/j.jsv.2019.01.037.

Balamurugan, V., and Narayanan, S. (2007), "A piezoelectric higher-order plate element for the analysis of multi-layer smart composite laminates", *Smart Mater. Struct.*, **16**(6), 2026-2039. http://dx.doi.org/10.1088/0964-1726/16/6/005.

Benjeddou, A. (2000) "Advances in piezoelectric finite element modeling of adaptive structural elements: a survey", *Comput. Struct.*, **76**(1-3), 347-363. https://doi.org/10.1016/S0045-7949(99)00151-0.

Benjeddou, A., and Deü, J.F. (2002a), "A two-dimensional closed-form solution for the free-vibrations analysis of piezoelectric sandwich plates", *Int. J. Solids Struct.*, **39**(6), 1463-1486. https://doi.org/10.1016/S0020-7683(01)00287-6.

Benjeddou, A., Deü, J.F., and Letombe, S. (2002b), "Free vibrations of simply-supported piezoelectric adaptive plates: an exact sandwich formulation", *Thin-Walled Struct.*, **40**(7-8), 573-593. https://doi.org/10.1016/S0263-8231(02)00013-7.

Bian, Z.G., Ying, J., Chen, W.Q., and Ding, H.J. (2006), "Bending and free vibration analysis of a smart functionally graded plate", *Struct. Eng. Mech.*, **23**(1), 97-113. https://doi.org/10.12989/sem.2006.23.1.097.

Birk, C., and Song, C. (2009), "A continued-fraction approach for transient diffusion in unbounded medium", *Comput. Meth. Appl. Mech. Eng.*, **198**(33-36), 2576-2590. https://doi.org/10.1016/j.cma.2009.03.002.

Carrera, E., and Nali, P. (2009), "Mixed piezoelectric plate elements with direct evaluation of transverse electric displacement", *Int. J. Numer. Methods Eng.*, **80**(4), 403-424. https://doi.org/10.1002/nme.2641.

Carrera, E., Büttner, A., and Nali, P. (2010a), "Mixed elements for the analysis of anisotropic multilayered piezoelectric plates", *J. Intell. Mater. Syst. Struct.*, **21**(7), 701-717. https://doi.org/10.1177/1045389X10364864.

Carrera, E., and Robaldo, A. (2010b), "Hierarchic finite elements based on a unified formulation for the static analysis of shear actuated multilayered piezoelectric plates", *Multidiscipline Modeling in Mater. Struct.*, **6**(1), 45-77. https://doi.org/10.1108/15736101011055266.

Cen, S., Soh, A.K., Long, Y.Q., and Yao, Z. H. (2002), "A new 4-node quadrilateral FE model with variable electrical degrees of freedom for the analysis of piezoelectric laminated composite plates", *Compos. Struct.*, **58**(4), 583-599. https://doi.org/10.1016/S0263-8223(02)00167-8.

Chen, D., Birk, C., Song, C., and Du, C. (2014), "A high-order approach for modelling transient wave propagation problems using the scaled boundary finite element method", *Int. J. Numer. Methods Eng.*, **97**(13), 937-959. https://doi.org/10.1002/nme.4613.

Cheung, Y.K., and Jiang, C.P. (2001), "Finite layer method in analyses of piezoelectric composite laminates", *Comput. Meth. Appl. Mech. Eng.*, **191**(8-10), 879-901. https://doi.org/10.1016/S0045-7825(01)00285-7.

Ding H.J., Xu R.Q., Chi Y.W., and Chen W.Q. (1999), "Free axisymmetric vibration of transversely isotropic piezoelectric circular plates", *Int. J. Solids Struct.*, **36**(30), 4629-4652. https://doi.org/10.1016/S0020-7683(98)00206-6.

Duan, W.H., Quek, S.T., and Wang, Q. (2005), "Free vibration analysis of piezoelectric coupled thin and thick annular plate", *J. Sound Vibr.*, **281**(1-2), 119-139. https://doi.org/10.1016/j.jsv.2004.01.009.

Dube, G.P., Upadhyay, M.M., Dumir, P.C., and Kumar, S. (1998), "Piezothermoelastic solution for angle-ply laminated plate in cylindrical bending", *Struct. Eng. Mech.*, **6**(5), 529-542. https://doi.org/10.12989/SEM.1998.6.5.529.

Garção, J.S., Soares, C.M., Soares, C.M., and Reddy, J.N. (2004), "Analysis of laminated adaptive plate structures using layerwise finite element models", *Comput. Struct.*, **82**(23-26), 1939-1959. https://doi.org/10.1016/j.compstruc.2003.10.024.

Ghasemabadian, M.A., and Saidi, A.R. (2017), "Stability analysis of transversely isotropic laminated Mindlin plates with piezoelectric layers using a Levy-type solution", *Struct. Eng. Mech.*, **62**(6), 675-693. https://doi.org/10.12989/SEM.2017.62.6.675.

Hashemi, S.H., Es'haghi, M., and Karimi, M. (2010), "Closed-form solution for free vibration of piezoelectric coupled annular plates using Levinson plate theory", *J. Sound Vibr.*, **329**(9), 1390-1408. https://doi.org/10.1016/j.jsv.2009.10.043.

Heyliger, P. (1994), "Static behavior of laminated elastic/piezoelectric plates", *AIAA J.*, **32**(12), 2481-2484. https://doi.org/10.2514/3.12321.

Heyliger, P., and Brooks, S. (1995a), "Free vibration of piezoelectric laminates in cylindrical bending", *Int. J. Solids Struct.*, **32**(20), 2945-2960. https://doi.org/10.1016/0020-7683(94)00270-7.

Heyliger, P., and Saravanos, D.A. (1995b), "Exact free-vibration analysis of laminated plates with embedded piezoelectric layers", *J. Acoust. Soc. Am.*, **98**(3), 1547-1557. https://doi.org/10.1121/1.413420.

Heyliger, P. (1997), "Exact solutions for simply supported laminated piezoelectric plates", *J. Appl. Mech.*, **64**(2), 299-306. https://doi.org/10.1115/1.2787307.

Heyliger, P.R., and Ramirez, G. (2000), "Free vibration of laminated circular piezoelectric plates and discs", *J. Sound Vibr.*, **229**(4), 935-956. https://doi.org/10.1006/jsvi.1999.2520.

Hosseini-Hashemi, S., Es'haghi, M., and Taher, H. R. D. (2010), "An exact analytical solution for freely vibrating piezoelectric coupled circular/annular thick plates using Reddy plate theory", *Compos. Struct.*, **92**(6), 1333-1351. https://doi.org/10.1016/j.compstruct.2009.11.006.

Kapuria, S. (2004), "A coupled zig-zag third-order theory for piezoelectric hybrid cross-ply plates", *J. Appl. Mech.*, **71**(5), 604-614. https://doi.org/10.1115/1.1767170.

Kapuria, S., and Kulkarni, S.D. (2008), "An efficient quadrilateral element based on improved zigzag theory for dynamic analysis of hybrid plates with electroded piezoelectric actuators and sensors", *J. Sound Vibr.*, **315**(1-2), 118-145. https://doi.org/10.1016/j.jsv.2008.01.053.

Kapuria, S., and Kulkarni, S.D. (2009), "Static electromechanical response of smart composite/sandwich plates using an efficient finite element with physical and electric nodes", *Int. J. Mech. Sci.*, **51**(1), 1-20. https://doi.org/10.1016/j.ijmecsci.2008.11.005.

Kapuria, S., Kumari, P., and Nath, J.K. (2010), "Efficient modeling of smart piezoelectric composite laminates: a review", *Acta Mech.*, **214**(1-2), 31-48. https://doi.org/10.1007/s00707-010-0310-0.

Khandelwal, R.P., Chakrabarti, A., and Bhargava, P. (2013), "An efficient hybrid plate model for accurate analysis of smart composite laminates", *J. Intell. Mater. Syst. Struct.*, **24**(16), 1927-1950. https://doi.org/10.1177/1045389X13486713.

Khandelwal, R.P., Chakrabarti, A., and Bhargava, P. (2014), "Static and dynamic control of smart composite laminates", *AIAA J.*, **52**(9), 1896-1914. https://doi.org/10.2514/1.J052666.

Kulikov, G.M., and Plotnikova, S.V. (2013), "Three-dimensional exact analysis of piezoelectric laminated plates via a sampling surfaces method", *Int. J. Solids Struct.*, **50**(11-12), 1916-1929. https://doi.org/10.1016/j.ijsolstr.2013.02.015.

Kulikov, G.M., and Plotnikova, S.V. (2017), "Benchmark solutions for the free vibration of layered piezoelectric plates based on a variational formulation", *J. Intell. Mater. Syst. Struct.*, **28**(19), 2688-2704. https://doi.org/10.1177/1045389X17698241.

Lage, R.G., Soares, C.M., Soares, C.M., and Reddy, J. N. (2004), "Modelling of piezolaminated plates using layerwise mixed finite elements", *Comput. Struct.*, **82**(23-26), 1849-1863. https://doi.org/10.1016/j.compstruc.2004.03.068.

Li, B., Fang, H., He, H., Yang, K., Chen, C., and Wang, F. (2019), "Numerical simulation and full-scale test on dynamic response of corroded concrete pipelines under Multi-field coupling", *Constr. Build. Mater.*, **200**, 368-386. https://doi.org/10.1016/j.conbuildmat.2018.12.111.

Li, C., Song, C., Man, H., Ooi, E.T., and Gao, W. (2014), "2D dynamic analysis of cracks and interface cracks in piezoelectric composites using the SBFEM", *Int. J. Solids Struct.*, **51**(11-12), 2096-2108. https://doi.org/10.1016/j.ijsolstr.2014.02.014.

Li, G., Dong, Z.Q., and Li, H.N. (2018), "Simplified Collapse-Prevention Evaluation for the Reserve System of Low-Ductility Steel Concentrically Braced Frames", *J. Struct. Eng.*, **144**(7), 04018071. https://doi.org/10.1061/(ASCE)ST.1943-541X.0002062.

Li, J., Shi, Z., and Ning, S. (2017), "A two-dimensional consistent approach for static and dynamic analyses of uniform beams", *Eng. Anal. Bound. Elem.*, **82**, 1-16. https://doi.org/10.1016/j.enganabound.2017.05.009.

Li, S., Huang, L., Jiang, L., and Qin, R. (2014), "A bidirectional B-spline finite point method for the analysis of piezoelectric laminated composite plates and its application in material parameter identification", *Compos. Struct.*, **107**, 346-362. https://doi.org/10.1016/j.compstruct.2013.08.007.

Lin, G., Zhang, P., Liu, J., and Li, J. (2018), "Analysis of laminated composite and sandwich plates based on the scaled boundary finite element method", *Compos. Struct.*, **187**, 579-592. https://doi.org/10.1016/j.compstruct.2017.11.001.

Liu, C.F., Chen, T.J., and Chen, Y.J. (2008), "A modified axisymmetric finite element for the 3-D vibration analysis of piezoelectric laminated circular and annular plates" *J. Sound Vibr.*, **309**(3-5), 794-804. https://doi.org/10.1016/j.jsv.2007.07.048.

Mackerle, J. (2003), "Smart materials and structures-a finite element approach-an addendum: a bibliography (1997–2002)", *Model. Simul. Mater. Sci. Eng.*, **11**(5), 707-744. https://doi.org/10.1088/0965-0393/11/5/302.

Man, H., Song, C., Gao, W., and Tin-Loi, F. (2012), "A unified 3D-based technique for plate bending analysis using scaled boundary finite element method", *Int. J. Numer. Methods Eng.*, **91**(5), 491-515. https://doi.org/10.1002/nme.4280.

Man, H., Song, C., Xiang, T., Gao, W., and Tin-Loi, F. (2013), "High-order plate bending analysis based on the scaled boundary finite element method", *Int. J. Numer. Methods Eng.*, **95**(4), 331-360. https://doi.org/10.1002/nme.4519.

Man, H., Song, C., Gao, W., and Tin-Loi, F. (2014), "Semi-analytical analysis for piezoelectric plate using the scaled boundary finite-element method", *Comput. Struct.*, **137**, 47-62. https://doi.org/10.1016/j.compstruc.2013.10.005.

Mauritsson, K., and Folkow, P.D. (2015), "Dynamic equations for a fully anisotropic piezoelectric rectangular plate", *Comput. Struct.*, **153**, 112-125. https://doi.org/10.1016/j.compstruc.2015.02.023.

Messina, A., and Carrera, E. (2015), "Three-dimensional free vibration of multi-layered piezoelectric plates through approximate and exact analyses", *J. Intell. Mater. Syst. Struct.*, **26**(5), 489-504. https://doi.org/10.1177/1045389X14529611.

Messina, A., and Carrera, E. (2016), "Three-dimensional analysis of freely vibrating multilayered piezoelectric plates through adaptive global piecewise-smooth functions", *J. Intell. Mater. Syst. Struct.*, **27**(20), 2862-2876. https://doi.org/10.1177/1045389X16642303.

Moleiro, F., Soares, C.M., Soares, C.M., and Reddy, J.N. (2012), "Assessment of a layerwise mixed least-squares model for analysis of multilayered piezoelectric composite plates", *Comput. Struct.*, **108**, 14-30. https://doi.org/10.1016/j.compstruc.2012.04.002.

Moleiro, F., Soares, C.M., Soares, C.M., and Reddy, J.N. (2014), "Benchmark exact solutions for the static analysis of multilayered piezoelectric composite plates using PVDF", *Compos. Struct.*, **107**, 389-395. https://doi.org/10.1016/j.compstruct.2013.08.019.

Moleiro, F., Soares, C.M., Soares, C.M., and Reddy, J. N. (2015), "Layerwise mixed models for analysis of multilayered piezoelectric composite plates using least-squares formulation", *Compos. Struct.*, **119**, 134-149. https://doi.org/10.1016/j.compstruct.2014.08.031.

Moleiro, F., Araújo, A.L., and Reddy, J.N. (2017), "Benchmark exact free vibration solutions for multilayered piezoelectric composite plates", *Compos. Struct.*, **182**, 598-605. https://doi.org/10.1016/j.compstruct.2017.09.035.

Pendhari, S.S., Sawarkar, S., and Desai, Y.M. (2015), "2D semi-analytical solutions for single layer piezoelectric laminate subjected to electro-mechanical loading", *Compos. Struct.*, **120**, 326-333. https://doi.org/10.1016/j.compstruct.2014.10.018.

Plagianakos, T.S., and Papadopoulos, E.G. (2015), "Higher-order 2-D/3-D layerwise mechanics and finite elements for composite and sandwich composite plates with piezoelectric layers", *Aerosp. Sci. Technol.*, **40**, 150-163. https://doi.org/10.1016/j.ast.2014.10.015.

Rezaiee-Pajand, M., and Sadeghi, Y. (2013), "A bending element for isotropic, multilayered and piezoelectric plates", *Lat. Am. J. Solids Struct.*, **10**(2), 323-348. http://dx.doi.org/10.1590/S1679-78252013000200006.

Saravanos, D.A., Heyliger, P.R., and Hopkins, D.A. (1997), "Layerwise mechanics and finite element for the dynamic analysis of piezoelectric composite plates", *Int. J. Solids Struct.*, **34**(3), 359-378. https://doi.org/10.1016/S0020-7683(96)00012-1.

Saravanos, D.A., and Heyliger, P.R. (1999), "Mechanics and computational models for laminated piezoelectric beams, plates, and shells", *Appl. Mech. Rev.*, **52**(10), 305-320. https://doi.org/10.1115/1.3098918.

Sawarkar, S., Pendhari, S., and Desai, Y. (2016), "Semi-analytical solutions for static analysis of piezoelectric laminates", *Compos. Struct.*, **153**, 242-252. https://doi.org/10.1016/j.compstruct.2016.05.106.

Shiyekar, S.M., and Kant, T. (2011), "Higher order shear deformation effects on analysis of laminates with piezoelectric fibre reinforced composite actuators", *Compos. Struct.*, **93**(12), 3252-3261. https://doi.org/10.1016/j.compstruct.2011.05.016.

Singh, A.K., Chaki, M.S., Hazra, B., and Mahto, S. (2017), "Influence of imperfectly bonded piezoelectric layer with irregularity on propagation of Love-type wave in a reinforced composite structure", *Struct. Eng. Mech.*, **62**(3), 325-344. https://doi.org/10.12989/SEM.2017.62.3.325.

Song, C., and Wolf, J.P. (1997), "The scaled boundary finite-element method-alias consistent infinitesimal finite-element cell method-for elastodynamics", *Comput. Meth. Appl. Mech. Eng.*, **147**(3-4), 329-355. https://doi.org/10.1016/S0045-7825(97)00021-2.

Song, C., and Wolf, J.P. (1999), "The scaled boundary finite element method-alias consistent infinitesimal finite element cell method-for diffusion", *Int. J. Numer. Methods Eng.*, **45**(10), 1403-1431. https://doi.org/10.1002/(SICI)1097-0207(19990810)45:10<1403::AID-NME636>3.0.CO;2-E.

Song, C., and Wolf, J.P. (2000), "The scaled boundary finite-element method-a primer: solution procedures", *Comput. Struct.*, **78**(1-3), 211-225. https://doi.org/10.1016/S0045-7949(00)00100-0.

Song, C., and Vrcelj, Z. (2008), "Evaluation of dynamic stress intensity factors and T-stress using the scaled boundary finite-element method", *Eng. Fract. Mech.*, **75**(8), 1960-1980. https://doi.org/10.1016/j.engfracmech.2007.11.009.

Song, C. (2009), "The scaled boundary finite element method in structural dynamics", *Int. J. Numer. Methods Eng.*, **77**(8), 1139-1171. https://doi.org/10.1002/nme.2454.

Song, C., Tin-Loi, F., and Gao, W. (2010), "A definition and evaluation procedure of generalized stress intensity factors at cracks and multi-material wedges", *Eng. Fract. Mech.*, **77**(12), 2316-2336. https://doi.org/10.1016/j.engfracmech.2010.04.032.

Tanzadeh, H., and Amoushahi, H. (2019), "Buckling and free vibration analysis of piezoelectric laminated composite plates using various plate deformation theories", *Eur. J. Mech. A-Solids*, **74**, 242-256. https://doi.org/10.1016/j.euromechsol.2018.11.013.

Torres, D.A.F., and Mendonça, P.T.R. (2010a), "Analysis of piezoelectric laminates by generalized finite element method and mixed layerwise-HSDT models", *Smart Mater. Struct.*, **19**(3), 035004. http://iopscience.iop.org/0964-1726/19/3/035004.

Torres, D.A.F., and Paulo de Tarso, R.M. (2010b), "HSDT-layerwise analytical solution for rectangular piezoelectric laminated plates", *Compos. Struct.*, **92**(8), 1763-1774. https://doi.org/10.1016/j.compstruct.2010.02.007.

Torres, D.A.F., Paulo de Tarso, R.M., and De Barcellos, C.S. (2011), "Evaluation and verification of an HSDT-Layerwise generalized finite element formulation for adaptive piezoelectric laminated plates", *Comput. Meth. Appl. Mech. Eng.*, **200**(5-8), 675-691. https://doi.org/10.1016/j.cma.2010.09.014.

Vel, S.S., Mewer, R.C., and Batra, R.C. (2004), "Analytical solution for the cylindrical bending vibration of piezoelectric composite plates", *Int. J. Solids Struct.*, **41**(5-6), 1625-1643. https://doi.org/10.1016/j.ijsolstr.2003.10.012.

Vidal, P., Gallimard, L., and Polit, O. (2016), "Modeling of piezoelectric plates with variables separation for static analysis", *Smart Mater. Struct.*, **25**(5), 055043. https://doi.org/10.1088/0964-1726/25/5/055043.

Wang, J., and Yang, J. (2000), "Higher-order theories of piezoelectric plates and applications", *Appl. Mech. Rev.*, **53**(4), 87-99. https://doi.org/10.1115/1.3097341.

Wolf, J.P., and Song, C. (2000), "The scaled boundary finite-element method-a primer: derivations", *Comput. Struct.*, **78**(1-3), 191-210. https://doi.org/10.1016/S0045-7949(00)00099-7.

Wu, L., Jiang, Z., and Feng, W. (2004), "An analytical solution for static analysis of a simply supported moderately thick sandwich piezoelectric plate", *Struct. Eng. Mech.*, **17**(5), 641-654. https://doi.org/10.12989/SEM.2004.17.5.641.

Wu, N., Wang, Q., and Quek, S.T. (2010), "Free vibration analysis of piezoelectric coupled circular plate with open circuit", *J. Sound Vibr.*, **329**(8), 1126-1136. https://doi.org/10.1016/j.jsv.2009.10.040.

Xiang, T., Natarajan, S., Man, H., Song, C., and Gao, W. (2014), "Free vibration and mechanical buckling of plates with in-plane material inhomogeneity-A three dimensional consistent approach", *Compos. Struct.*, **118**, 634-642. https://doi.org/10.1016/j.compstruct.2014.07.043.

Zhang, P., Qi, C., Fang, H., Ma, C., and Huang, Y. (2019), "Semi-analytical analysis of static and dynamic responses for laminated magneto-electro-elastic plates", *Compos. Struct.*, **222**, 110933. https://doi.org/10.1016/j.compstruct.2019.110933.

Zhang, P., Qi, C., Fang, H., and He, W. (2020), "Three dimensional mechanical behaviors of in-plane functionally graded plates", *Compos. Struct.*, 112124. https://doi.org/10.1016/j.compstruct.2020.112124.

Zhang, Z., Feng, C., and Liew, K.M. (2006), "Three-dimensional vibration analysis of multilayered piezoelectric composite plates", *Int. J. Eng. Sci.*, **44**(7), 397-408. https://doi.org/10.1016/j.ijengsci.2006.02.002.

Zhong, W.X., Lin, J.H., and Gao, Q. (2004), "The precise computation for wave propagation in stratified materials", *Int. J. Numer. Methods Eng.*, **60**(1), 11-25. https://doi.org/10.1002/nme.952.

CC

Appendix. Coefficients of the matrix [*Q*]

The coefficient conversions from the matrix [C] in the local fiber coordinate system to [Q] in the global Cartesian coordinate system are listed in the following:

$$Q_{11} = c_{11}c^4 + 2(c_{12} + 2c_{45})s^2c^2 + c_{22}s^4 \quad \text{(A.1)}$$

$$Q_{12} = c_{12}\left(c^4 + s^4\right) + (c_{11} + c_{22} - 4c_{45})s^2c^2 \quad \text{(A.2)}$$

$$Q_{13} = c_{13}c^2 + c_{23}s^2 \quad \text{(A.3)}$$

$$Q_{14} = (c_{11} - c_{12} - 2c_{45})sc^3 + (c_{12} - c_{22} + 2c_{45})cs^3 \quad \text{(A.4)}$$

$$Q_{22} = c_{11}s^4 + 2(c_{12} + 2c_{45})s^2c^2 + c_{22}c^4 \quad \text{(A.5)}$$

$$Q_{23} = c_{13}s^2 + c_{23}c^2 \quad \text{(A.6)}$$

$$Q_{24} = (c_{11} - c_{12} - 2c_{45})s^3c + (c_{12} - c_{22} + 2c_{45})c^3s \quad \text{(A.7)}$$

$$Q_{33} = c_{33} \quad \text{(A.8)}$$

$$Q_{34} = (c_{13} - c_{23})sc \quad \text{(A.9)}$$

$$Q_{44} = (c_{11} - 2c_{12} + c_{22} - 2c_{45})c^2s^2 + c_{45}\left(c^4 + s^4\right) \quad \text{(A.10)}$$

$$Q_{55} = c_{56}c^2 + c_{46}s^2 \quad \text{(A.11)}$$

$$Q_{56} = (c_{46} - c_{56})sc \quad \text{(A.12)}$$

$$Q_{66} = c_{46}c^2 + c_{56}s^2 \quad \text{(A.13)}$$

$$\bar{e}_{31} = e_{31}c^2 + e_{32}s^2 \quad \text{(A.14)}$$

$$\bar{e}_{32} = e_{31}s^2 + e_{32}c^2 \quad \text{(A.15)}$$

$$\bar{e}_{33} = e_{33} \quad \text{(A.16)}$$

$$\bar{e}_{34} = (e_{31} - e_{32})sc \quad \text{(A.17)}$$

$$\bar{e}_{15} = (e_{15} - e_{24})sc \quad \text{(A.18)}$$

$$\bar{e}_{16} = e_{15}c^2 + e_{24}s^2 \quad \text{(A.19)}$$

$$\bar{e}_{25} = e_{24}c^2 + e_{15}s^2 \quad \text{(A.20)}$$

$$\bar{e}_{26} = (e_{15} - e_{24})sc \quad \text{(A.21)}$$

$$\nu_{xx} = \nu_{11}c^2 + \nu_{22}s^2 \quad \text{(A.22)}$$

$$\nu_{yy} = \nu_{11}s^2 + \nu_{22}c^2 \quad \text{(A.23)}$$

$$\nu_{xy} = (\nu_{11} - \nu_{22})sc \quad \text{(A.24)}$$

$$\nu_{zz} = \nu_{33} \quad \text{(A.25)}$$

in which c and s stand for $c=\cos\alpha$ and $s=\sin\alpha$ with the angle α measured anticlockwise from the x-axis to the 1-axis.